Redox Biology 67 (2023) 102871

Contents lists available at ScienceDirect

Redox Biology

journal homepage: www.elsevier.com/locate/redox

Mesenchymal stem cell attenuates spinal cord injury by inhibiting mitochondrial quality control-associated neuronal ferroptosis

Senyu Yao [a,b,c,d,1], Mao Pang [a,c,d,1], Yanheng Wang [b,1], Xiaokang Wang [a,c,d,1], Yaobang Lin [b], Yanyan Lv [b], Ziqi Xie [b], Jianfeng Hou [e], Cong Du [c,f], Yuan Qiu [b], Yuanjun Guan [g], Bin Liu [a,c,d,****], Jiancheng Wang [b,h,i,***], Andy Peng Xiang [b,j,k,**], Limin Rong [a,c,d,*]

[a] Department of Spine Surgery, The Third Affiliated Hospital of Sun Yat-Sen University, Guangzhou, 510630, China
[b] Center for Stem Cell Biology and Tissue Engineering, Key Laboratory for Stem Cells and Tissue Engineering, Ministry of Education, Sun Yat-Sen University, Guangzhou, 510275, China
[c] National Medical Products Administration (NMPA) Key Laboratory for Quality Research and Evaluation of Cell Products, The Third Affiliated Hospital of Sun Yat-Sen University, Guangzhou, 510630, China
[d] Guangdong Engineering Technology Research Center of Minimally Invasive Spine Surgery, The Third Affiliated Hospital of Sun Yat-Sen University, Guangzhou, 510630, China
[e] Department of Joint and Trauma Surgery, The Third Affiliated Hospital of Sun Yat-sen University, Guangzhou, 510630, China
[f] Cell-Gene Therapy Translational Medicine Research Center, The Third Affiliated Hospital of Sun Yat-Sen University, 510630, Guangzhou, China
[g] Core Facility of Center, Zhongshan School of Medicine, Sun Yat-Sen University, Guangzhou, 510275, China
[h] Scientific Research Center, The Seventh Affiliated Hospital of Sun Yat-sen University, Shenzhen, 518107, China
[i] Department of Hematology, The Seventh Affiliated Hospital, Sun Yat-Sen University, Shenzhen, 518107, China
[j] Department of Biochemistry, Zhongshan School of Medicine, Sun Yat-Sen University, Guangzhou, 510275, China
[k] Center for Precision Medicine, Sun Yat-Sen University, Guangzhou, 510275, China

ARTICLE INFO

Keywords:
Neuronal ferroptosis
Mitochondrial quality control
Intercellular mitochondrial transfer
Mesenchymal stem cells
Spinal cord injury

ABSTRACT

Ferroptosis is a newly discovered form of iron-dependent oxidative cell death and drives the loss of neurons in spinal cord injury (SCI). Mitochondrial damage is a critical contributor to neuronal death, while mitochondrial quality control (MQC) is an essential process for maintaining mitochondrial homeostasis to promote neuronal survival. However, the role of MQC in neuronal ferroptosis has not been clearly elucidated. Here, we further demonstrate that neurons primarily suffer from ferroptosis in SCI at the single-cell RNA sequencing level. Mechanistically, disordered MQC aggravates ferroptosis through excessive mitochondrial fission and mitophagy. Furthermore, mesenchymal stem cells (MSCs)-mediated mitochondrial transfer restores neuronal mitochondria pool and inhibits ferroptosis through mitochondrial fusion by intercellular tunneling nanotubes. Collectively, these results not only suggest that neuronal ferroptosis is regulated in an MQC-dependent manner, but also fulfill the molecular mechanism by which MSCs attenuate neuronal ferroptosis at the subcellular organelle level. More importantly, it provides a promising clinical translation strategy based on stem cell-mediated mitochondrial therapy for mitochondria-related central nervous system disorders.

1. Introduction

Spinal cord injury (SCI) is a highly crippling traumatic disorder of central nervous system (CNS) with poor prognosis and affects approximately 15–40 people per million around the world, which has rapidly increased with the development of modern society [1,2]. Despite the

* Corresponding author. Department of Spine Surgery, The Third Affiliated Hospital of Sun Yat-Sen University, Guangzhou, 510630, China.
** Corresponding author. Center for Stem Cell Biology and Tissue Engineering, Key Laboratory for Stem Cells and Tissue Engineering, Ministry of Education, Sun Yat-Sen University, Guangzhou, 510275, China.
*** Corresponding author. Scientific Research Center, The Seventh Affiliated Hospital of Sun Yat-sen University, Shenzhen, 518107, China.
**** Corresponding author. Department of Spine Surgery, The Third Affiliated Hospital of Sun Yat-Sen University, Guangzhou, 510630, China.
E-mail addresses: liubin6@mail.sysu.edu.cn (B. Liu), wangjch38@mail.sysu.edu.cn (J. Wang), xiangp@mail.sysu.edu.cn (A.P. Xiang), ronglm@mail.sysu.edu.cn (L. Rong).
[1] These authors contributed equally: Senyu Yao, Mao Pang, Yanheng Wang, Xiaokang Wang.

https://doi.org/10.1016/j.redox.2023.102871
Received 17 August 2023; Accepted 31 August 2023
Available online 7 September 2023

accumulating advancement of basic and clinical research in recent years, a failure of effective neural regeneration after SCI remains critical limitations for achieving neural function restoration [3,4].

SCI is caused by the irreversible primary injury from mechanical forces followed by cascading reactions known as the secondary injury, including local hemorrhage, ischemia, hypoxia, ionic imbalance, free radical stress [5]. In particular, it was highlighted that oxidative stress caused by excessive reactive oxygen species (ROS) production in the acute and (or) subacute phase of the secondary injury largely reduces the viability of neurons, which subsequently impedes the neural regeneration [3,5,6].

Recently, mounting experimental evidence demonstrates that ferroptosis, a unique modality of non-apoptotic regulated oxidative cell death characterized by iron-dependent lipid peroxidation [7] plays a critical role in various neurological diseases, including traumatic CNS injuries like SCI [8–11]. Actually, neurons are intrinsically susceptible to the oxidative stress because of abundant polyunsaturated fatty acid residues in the neuronal phospholipid membrane and poor capacity of scavenging ROS [12–14]. Together, these findings suggest that targeting neuronal ferroptosis could be an ideal approach to enhance neuronal survival [15–17], thus promoting the recovery of motor dysfunction in SCI. However, up to date, research on ferroptosis is mainly limited to a single molecular target or mechanism on iron metabolism or redox system via small molecule compounds [18–20], while it is unclear about the modulatory mechanisms at the suborganelle level and also lack of possibility of clinical transformation.

Mitochondria, the core of oxidative metabolism, play a vital role in maintaining the redox homeostasis [5,21,22], were reported to participate in ferroptosis extensively via orchestration of iron homeostasis, energy metabolism, lipid synthesis [23–25]. For the systemic regulation of mitochondrial function, mitochondrial quality control (MQC) has to be highlighted, which describes the processes by which cells response to internal and external stresses involving mitochondria-nuclear crosstalk and remodeling of mitochondrial network via mitochondrial dynamics as well as mitophagy at the organelle level [26,27]. In fact, previous studies partly revealed the role of MQC in neurological diseases, like optic neuropathies and cerebral ischemia-reperfusion injury [28,29]. Therefore, revealing the function of MQC in regulating mitochondrial homeostasis and neuronal ferroptosis will provide new insights into therapies for mitochondria-related CNS diseases.

Furthermore, at the aspect of clinical transformation, a new pattern of mitochondrial therapy by exogenous supplement of healthy mitochondria into cells was proposed and exhibited a promising outcome in CNS trauma like traumatic brain injury and SCI [30]. But the problems are that purified mitochondrial transplantation failed to accurately target the damaged neurons and lacked long-lasting functional improvement of neural function in SCI [30,31]. Recently, more and more studies have considered mesenchymal stem cells (MSCs) as a potential therapeutic delivery vectors to transfer their mitochondria to unhealthy cells and rescue the tissue injury in various neurological diseases [32]. However, there are no systematic studies on the mechanism of mitochondrial transfer between MSCs and neurons in the treatment of SCI.

Here, we further analyzed the role of ferroptosis in spinal neurons after SCI at the single-cell RNA sequencing level, and found that dysregulated mitochondrial quality control mediated the neuronal ferroptosis by imbalanced mitochondrial dynamics and excessive mitophagy. Furthermore, we proposed that MSCs can be a satisfactory candidate for mitochondrial transplantation-based therapy of SCI by transferring mitochondria to neurons via intracellular tunneling nanotubes-mediated direct cell-to-cell contact. The delivered mitochondria restored the mitochondrial homeostasis by fusing with neuronal mitochondria, thus inhibiting mitochondrial fission and mitophagy, and finally attenuated the neuronal ferroptosis. Moreover, in vivo experiments showed that MSCs could effectively inhibit ferroptosis and improve functional recovery after SCI through mitochondrial transfer. Our results offered novel insights into MQC-dependent neuronal ferroptosis and provided a promising clinical translation strategy based on stem cell-mediated mitochondrial therapy for mitochondria-related CNS disorders.

2. Results

2.1. Neurons suffer from ferroptosis after spinal cord injury

To determine the intrinsic reason for neuronal death after spinal cord injury (SCI), we deeply investigated pathophysiological changes that occurred in neurons during SCI by analyzing the single-cell RNA sequencing data from Li et al. [33]. We found that the cell proportion of neurons decreased most significantly after SCI, which was evidenced by H&E and Nissl staining histological analysis showing inapparent nuclei and smaller Nissl bodies (Fig. 1A–E and Supplementary Fig. 1A). The significant reduction in the neuron population suggested that early intervention targeting neuron survival may benefit neural function recovery.

It is well known that the oxidative stress may activate multiple mechanisms of cell death [34]. Furthermore, large amounts of ROS was produced during the acute phase of SCI, which suggested that the loss of neurons was related to oxidative damage in SCI [5]. Therefore, we assessed the expression levels of multiple genes associated with classical types of cell death in neurons after SCI. Remarkably, neurons exhibited the enrichment of genes associated with oxidative stress, ferroptosis and lipid metabolic process after SCI (Fig. 1F). Moreover, the alteration of typical gene expression profile after SCI showed the ferroptotic drivers were more highly expressed in the SCI group, whereas ferroptotic suppressors were more abundant in the uninjured group (Fig. 1G–H). Furthermore, our result also demonstrated that neurons were more prone to suffer ferroptosis than other neural cells (Supplementary Figs. 2A–D). In accordance with our findings, a spatiotemporal transcriptome analysis of scar tissue after SCI also found that gene expression of ferroptosis in neurons was peaked at the injury center throughout 28 days after SCI [35]. On the other hand, to investigate the significance of ferroptosis in neuronal cell death in comparison to other modality of regulated cell death, we analyzed the expression level of typical genes marking apoptosis, necroptosis and pyroptosis. We found that compared with the sham group, only the expression of ferroptosis-related genes significantly increased in SCI group. (Supplementary Fig. 1B). These results indicated that ferroptosis may primarily contribute to the neuronal death after SCI.

Then we further verified the features of the ferroptotic neurons after SCI in vivo. We established the crush injury model that typically resembles the ischemia and hypoxia microenvironment in SCI. The morphological characteristic of mitochondria is widely acknowledged as the gold hallmark of ferroptosis [7,22,23]. Accordingly, we found that after SCI, mitochondria in neurons shrunk with condensed inner membrane and diminished cristae under transmission electron microscope (Fig. 1I–K). Immunofluorescence staining showed that TFRC, the transferrin receptor that is necessary for cellular iron uptake, were about 4-fold more abundant in the SCI group than in the sham group. The higher accumulation of 4-HNE, a marker of lipid peroxidation, also represented the occurrence of ferroptosis after SCI (Fig. 1L-O). Taken together, these results indicated that the neurons suffered from ferroptosis mostly after SCI.

2.2. Neurons exhibit disordered mitochondrial quality control during ferroptosis

Mitochondria are core organelles responsible for maintaining cell survival, redox homeostasis, iron metabolism and closely related with the development of oxidative stress-induced ferroptosis [36]. More importantly, neurons are highly dependent on mitochondrial respiration for energy source, which highlights the role of mitochondria in

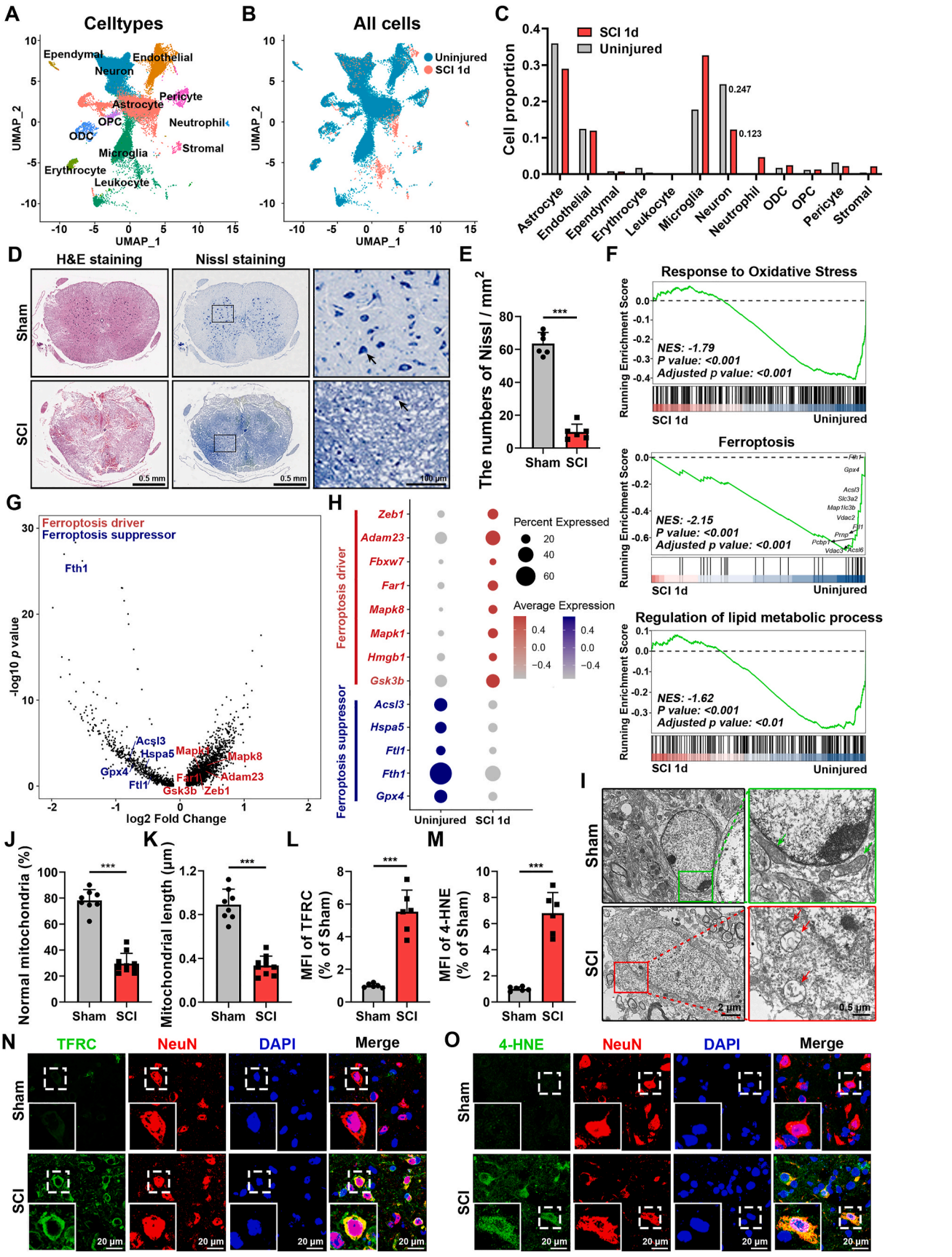

(caption on next page)

Fig. 1. Neurons exhibit ferroptosis after spinal cord injury. (A) Cell clusters of the sc-RNA-seq data from Li et al. in figshare with the identifier (https://doi.org/10.6084/m9.figshare.17702045). (B) UMAP plot of all cells of the scRNA-seq data in **(A)**. (C) Quantitative analysis of the proportion of each cell in **(B)**. (D) Representative Hematoxylin and eosin (H&E) and Nissl staining of spinal cord from mice induced by sham or crush injury surgery (1 day after SCI). Scale bar, 0.5 μm for original pictures and 100 μm for enlarged pictures. (E) Quantification for the numbers of Nissl per square milimeter (mm^2) in (B). (n=6 biological repeats for each group; Unpaired *t*-test). (F) The GSEA of the hallmark gene sets in MSigDB database revealing the enrichment of response to oxidative stress, ferroptosis and regulation of lipid metabolic process GO terms in neurons. NES, normalized enrichment score. (G) The scatter plot of the ferroptosis-related genes in neurons. (H) The dot plot showing the differentially expressed genes in neurons between the uninjured and injured spinal cord. (I) Representative transmission electron microscope (TEM) images of neurons from mice induced by sham or crush injury surgery (1 day after SCI) in vivo. Red and green arrows indicate damaged and normal mitochondria respectively. Scale bar, 2 μm for original pictures and 0.5 μm for enlarged pictures. (J) Quantitative analysis of percentage of mitochondria with normal morphology in **(I)**. (n = 8 biological repeats for Sham group and n=10 biological repeats for SCI group; Unpaired *t*-test). (K) Quantitative analysis of average value of mitochondrial length (micrometers, μm) in **(D)**. (n = 8 biological repeats for Sham group and n=10 biological repeats for SCI group; Unpaired *t*-test). (L–M) Quantification of mean fluorescence intensity of ferroptosis-related markers in **(N–O)**. (n = 6 biological repeats for each group; Unpaired *t*-test). (N–O) Representative confocal images of neurons, stained with ferroptosis-related markers, such as TFRC and 4-HNE, of spinal cord from mice induced by sham or crush injury surgery (1 day after SCI) in vivo. Neurons were marked by NeuN. Scale bar, 20 μm. Two-sided comparison; All data are mean ± SD; Error bars represent SDs; ***$p < 0.001$; See also Supplementary Figs. 1 and 2. (For interpretation of the references to colour in this figure legend, the reader is referred to the Web version of this article.)

ferroptosis-related CNS diseases. Mitochondrial quality control (MQC) is indispensable in maintaining mitochondrial homeostasis to ensure that there are requisite number of functional mitochondria to meet the demand of cells, especially under stress [37]. MQC involves mitochondria-nuclear crosstalk and mitochondrial network remodeling at the organelle level via mitochondrial dynamics as well as mitophagy [37]. However, whether mitochondrial dynamics and mitophagy-mediated MQC modulates neuronal ferroptosis is not fully elucidated. Therefore, to explore the change of MQC, we applied the super-resolution microscope (HIS-SIM) for dynamically tracking the fate of mitochondria in alive Ht22 cells (mouse primary hippocampal neurons) after using (1S,3R)-RSL3 (Rsl3, a Gpx4 inhibitor) to induce ferroptosis. Remarkably, we found that excessive mitochondria became dotted and then integrated with lysosomes (Fig. 2A–B and Supplementary Video 1), which represented the process of mitophagy following mitochondrial fission. We also found that the mitochondrial activity significantly decreased (Supplementary Figs. 3A–B). The above results revealed disordered MQC in neurons during ferroptosis.

Supplementary video related to this article can be found at https://doi.org/10.1016/j.redox.2023.102871

Furthermore, we deeply investigated the change associated with mitochondrial dynamics and mitophagy in ferroptotic neurons. We observed that the morphology of mitochondrial network appeared fragmented when Ht22 cells were exposed to Rsl3-induced ferroptosis (Fig. 2C–F), which was confirmed by the enhanced expression of proteins participating in mitochondrial fission and reduced expression of proteins associated with mitochondrial fusion (Fig. 2G and Supplementary Figs. 3C–G). Additionally, ferroptosis is considered as a type of autophagy-dependent cell death and several types of selective autophagy drive the development of ferroptosis [38,39]. However, the relationship between mitophagy and ferroptosis has not been elucidated clearly. Thus, we next detected the ferroptosis-related change in mitophagy and found excessive level of mitophagy during ferroptosis than control group (Fig. 2H-L and Supplementary Figs. 3H–I), which were also consistent with our previous results. Regarding the mitochondrial functions, there were an obvious increase in mitochondrial ROS and declines in mitochondrial membrane potential and ATP production in ferroptotic neurons, indicating imbalanced mitochondrial homeostasis (Fig. 2M-Q). To sum up, our results demonstrated that ferroptosis developed in the MQC-dependent manner and the MQC in ferroptotic neurons was too deteriorated to compensate the holistic mitochondrial network and led to mitochondrial dysfunction.

2.3. MSCs infuse functional mitochondria into ferroptotic neurons via TNT

Given that oxidative stress associated with mitochondria damage is thought to contribute to the risk of neuronal death in SCI, we hypothesized that mesenchymal stem cell (MSC) therapy, which exerts potent antioxidant and cytoprotective effects, could be a potential solution [40]. Besides, the transfer of mitochondria was reported to be one mechanism by which the MSCs work to improve the tissue repair and involve in many biological processes in health and disease [32]. Here, we successfully isolated MSCs from the human umbilical cord (Supplementary Figs. 4A–B), and speculated that they could alleviate neuronal ferroptosis by the delivery of mitochondria. Thus, to determine whether mitochondrial transfer occurred between MSCs and Ht22 cells, we developed an MSC-Ht22 coculture system under stimulation of ferroptosis inducer, Rsl3. The mitochondria of MSCs were tracked by labelling them with mitochondria specific dye, Mitotracker and Celltracker was also used to distinguish Ht22 cells in the coculture system (Fig. 3A). First, we performed confocal microscopy and directly observed mitochondrial transfer between MSCs and Ht22 cells. Meanwhile, Rsl3 could trigger increased mitochondria exchange (Fig. 3B and Supplementary Figs. 5A–B). Interestingly, we also found that there was a prominent increase of MSC-derived mitochondria in Ht22 cells along with time (Fig. 3C–D and Supplementary Fig. 5C). Moreover, the result of the confocal microscopy was consistent with our previous results (Supplementary Figs. 5D–E). To further confirm the mitochondrial transfer, we labeled MSC-derived mitochondria with green fluorescent protein (GFP) by lentiviral transduction and also observed the same phenomena (Supplementary Figs. 5F–I). Taken together, these results showed that MSCs could transfer mitochondria to Ht22 cells under Rsl3-induced ferroptosis.

Mitochondrial transfer between cells has been reported to be mediated by tunneling nanotubes (TNTs), microvesicles and gap junction [41]. In our study, mitochondrial transfer between MSCs and neurons through TNTs was confirmed at the nanoscale by scanning electron microscopy and confocal microscopy also showed the presence of TNT containing mitochondria in it (Fig. 3E–H). Then, to further confirm the mechanism, 18-α-GA (a blocker of gap junctions), the dynamin inhibitor Dynasore (a blocker of microvesicle endocytosis), and the potent actin polymerization inhibitor cytochalasin D (Cyto D, a blocker of TNT formation) were added to the coculture system with Rsl3. Mitochondrial transfer was then analyzed with flow cytometry and we observed that, compared with Control group, Cyto D significantly inhibited mitochondrial transfer form MSCs to Ht22 cells, whereas 18-α-GA or Dynasore treatment had no significant effect (Supplementary Figs. 6A–D). Therefore, these data show that TNTs are the key mechanism by which mitochondria were transfer from MSCs to Ht22 cells under ferroptotic stimulation.

2.4. MSC-mediated mitochondrial transfer stabilizes mitochondrial quality control in ferroptotic neurons

To further investigate whether MSC-derived mitochondria could restore the distorted MQC during neuronal ferroptosis, we first detected the mitochondrial activity in Ht22 cells and found that Ht22 cells lost

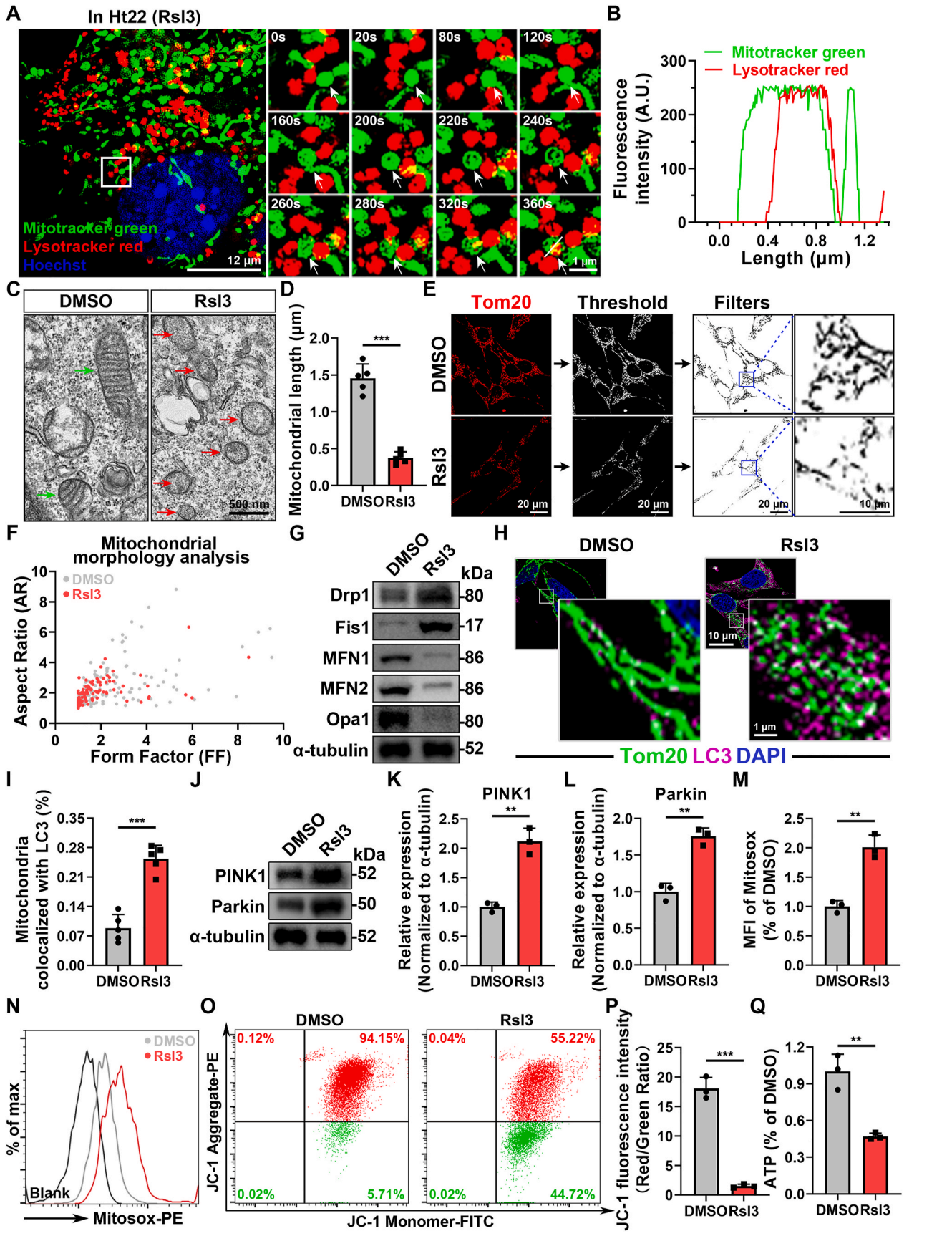

(caption on next page)

Fig. 2. Neurons exhibit disordered mitochondrial quality control during ferroptosis. (A) Representative super-resolution living cell tracing images of mitophagy in Ht22 cells after Rsl3 treatment for 12 h at different time points. Mitochondria were stained with Mitotracker green and Lysosome were stained with Lysotracker red. Corresponding video is provided as a Source Data file. Scale bar, 12 μm for original pictures and 1 μm for enlarged pictures. (B) Colocalization analysis of the fluorescence intensity of the white line area in **(A)**. (C) Representative TEM images of the morphology of mitochondria in Ht22 cells after treated with DMSO or Rsl3 for 24 h. Red and green arrows indicate damaged and normal mitochondria respectively. Scale bar, 500 nm. (D) Quantitative analysis of average value of mitochondrial length (μm) in **(C)**. (n=3 biological repeats for each group; N = 28–40 mitochondria; Unpaired *t*-test). (E) Representative immunostaining pictures of mitochondrial morphology of Ht22 cells after treated with DMSO or Rsl3 for 24 h. Mitochondrial outer membranes were marked by Tom20. Scale bar, 20 μm for original pictures and 10 μm for enlarged pictures. (F) A plot of Aspect Ratio (AR) against Form Factor (FF) shows that particles in **(E)**. (G) Western Blot analysis of the proteins associated with mitochondrial fusion and fission in Ht22 cells after treated with DMSO or Rsl3 for 24 h. (H) Representative immunostaining pictures of mitophagy potential in Ht22 cells after treated with DMSO or Rsl3 for 24 h. Mitochondrial outer membranes were marked with Tom20 and autophagy was marked with LC3, respectively. Scale bar, 10 μm for original pictures and 1 μm for enlarged pictures. (I) Quantification of the average level of colocalization between mitochondria and LC3 in **(H)**. (n=5 biological repeats for each group; Unpaired *t*-test). (J) Western Blot analysis of mitophagy related proteins, such as PINK1 and Parkin, in Ht22 cells after treated with DMSO or Rsl3 for 24 h. (K–L) Quantitative analysis of the expression of mitophagy related proteins, such as PINK1 and Parkin in **(J)**. (n=3 biological repeats for each group; Unpaired *t*-test) (M−N) Flow cytometry and quantitative analysis of the mean fluorescence intensity of mitochondrial ROS level in Ht22 cells after treated with DMSO or Rsl3 for 24 h. Mitochondrial ROS was probed with Mitosox (PE channel), (n=3 biological repeats for each group; Unpaired *t*-test). (O) Flow cytometry analysis of mitochondrial membrane potential (MMP) probed with JC-1 in Ht22 cells after treated with DMSO or Rsl3 for 24 h. (P) Quantitative analysis of the ratio of JC-1 aggregates (referred to high MMP, PE channel) /JC-1 monomers (referred to low MMP, FITC channel) in **(O)**. (n=3 biological repeats for each group; Unpaired *t*-test). (Q) Measurement of the intracellular ATP level in Ht22 cells after treated with DMSO or Rsl3 for 24 h (n=3 biological repeats for each group; Unpaired *t*-test) Two-sided comparison; All data are mean ± SD; Error bars represent SDs; $^{**}p < 0.01$, $^{***}p < 0.001$; See also Supplementary Fig. 3. (For interpretation of the references to colour in this figure legend, the reader is referred to the Web version of this article.)

their functional mitochondrial mass under Rsl3 stimulation, and yet this was restored by coculture with MSCs (Fig. 4A and Supplementary Fig. 7A), indicating the recovery of imbalanced mitochondrial homeostasis after MSC therapy. Then, we labeled and tracked MSC-derived mitochondria. Surprisingly, we found that they were colocalized with resident mitochondria in Ht22 cells, indicating that MSC coculture promotes mitochondrial fusion in Ht22 cells during ferroptosis (Fig. 4B). To further confirm the improvement of mitochondria dynamics, we used transmission electron microscope and confocal microscope to observe the morphology of mitochondria. Consistent with the results of western blot analysis of mitochondrial dynamics-related proteins, we identified that mitochondria in Ht22 cells became longer after coculture with MSCs under the stimulation of ferroptosis (Fig. 4C and Supplementary Figs. 7B–J). Furthermore, we found that MSC coculture could also reduce excessive mitophagy during ferroptosis (Fig. 4D–F and Supplementary Fig. 7K-L). Additionally, regarding mitochondrial functions, we observed that MSC coculture recovered not only the increase in mitochondrial ROS, but also the obvious declines in mitochondrial membrane potential and ATP production under ferroptosis, indicating balanced mitochondrial homeostasis was achieved (Fig. 4G–K). Together, these findings verified our conclusion that MSC coculture regulates MQC and improves mitochondrial homeostasis in ferroptotic neurons.

2.5. Inhibition of mitochondrial transfer impedes the recovery of mitochondrial quality control mediated by MSCs during neuronal ferroptosis

To further clarify whether MSCs provide protection for stabilizing mitochondrial homeostasis through mitochondrial transfer, we applied corresponding loss-of-function experiments and results showed that the process of mitochondrial transfer from MSCs was blocked using TNT formation inhibitor Cyto D (Fig. 5A–B). Next, we observed mitochondria became fragmented and smaller after Cyto D treatment, suggesting the balance of mitochondrial fission and fusion was broken, which was confirmed by living cell tracing, western blot, immunofluorescence staining and transmission electron microscope (Supplementary Fig. 8A-L). Excessive mitophagy was also showed by increased number of autolysosomes that contain mitochondria, along with elevated mitophagy-associated markers expression (Fig. 5C–G and Supplementary Fig. 8M−N). Besides, we further revealed disturbed mitochondria functions featured by increased mitochondrial ROS, lower mitochondrial membrane potential and reduced ATP production (Fig. 5H-L). Altogether, these results indicate that MSC-mediated mitochondrial transfer regulates MQC and improves mitochondrial homeostasis in ferroptotic neurons.

2.6. MSC coculture inhibits neuronal ferroptosis through mitochondrial transfer

Next, we further investigated whether MSCs could suppress neuronal ferroptosis through mitochondrial transfer. By analyzing the expression of ferroptosis-related markers, we identified direct neuroprotective effect of MSCs on inhibiting neuronal ferroptosis in Ht22 cells (Fig. 6A–B and Supplementary Figs. 9A–D). Meanwhile, at the biochemical levels, ferroptosis is an iron-dependent form of nonapoptotic cell death caused by lipid peroxide overload on biological membranes [42]. Accordingly, we observed that there was a decrease in intracellular ROS levels, especially lipid ROS, as well as reduced malondialdehyde (MDA), which is a representative product of lipid peroxidation, after cocultured with MSCs (Fig. 6C–H). Additionally, there was an obvious decline in intercellular total iron and free Fe^{2+} levels in the coculture system. (Fig. 6I–K). Altogether, these data demonstrated that MSC coculture provides a neuroprotective effect for neurons from ferroptosis, which is the main form of neuronal death during SCI.

We next applied Cyto D treatment in coculture system to investigate whether MSCs inhibited neuronal ferroptosis through mitochondrial transfer. The results showed that Ht22 cells displayed significant ferroptosis phenotype at the molecular level upon Cyto D treatment. (Supplementary Figs. 10A–F). Additionally, at the biochemical level, Cyto D treatment resulted in an increase in intracellular ROS levels, especially lipid ROS, and more malondialdehyde (MDA) production (Supplementary Fig. 10G-L). Additionally, we further detected the intercellular total iron and free Fe^{2+} levels and found that the iron content was increased in the coculture system. (Supplementary Fig. 10M−O). These findings confirmed that MSCs inhibit neuronal ferroptosis via the mitochondrial transfer-dependent pathway.

2.7. MSC transplantation alleviates neuronal ferroptosis and promotes functional recovery after SCI by delivery of mitochondria

To further examine the role of MSCs in the development of SCI in vivo, we constructed SCI crush injury mice and transplanted MSCs that were pre-treated with or without Cyto D, into the crush injury epicenter (Fig. 7A). By tracing of mitochondria from injected MSCs in vivo, interestingly, we observed MSC-derived mitochondria appeared in the neurons after SCI, indicating MSCs have a potency of transferring mitochondria to spinal neurons after SCI (Fig. 7B).

Furthermore, we investigated the effect of MSC therapy for treating SCI, and found that neurons exhibited decreased ferroptosis markers expression with more intact and longer mitochondria, and consequently there was an increasing number of neurons compared to the SCI group, which failed to be rescued by Cyto D pre-treatment (Fig. 7C and

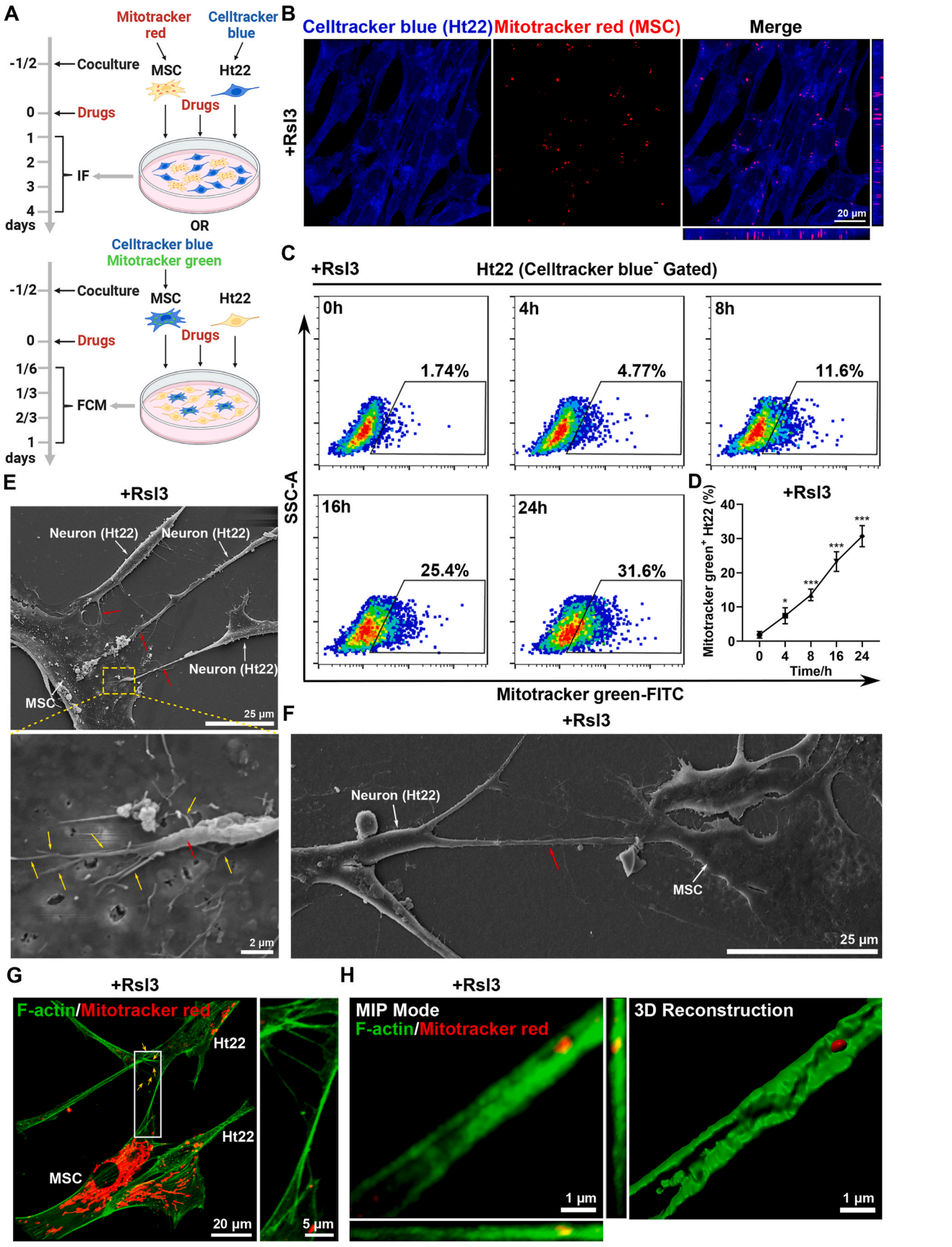

(caption on next page)

Fig. 3. MSCs infuse functional mitochondria into ferroptotic neurons via TNT. (A) Schematic diagram of MSC-Ht22 coculture system. Flow cytometry (FCM) of Mitotracker green uptake by Ht22 cells cocultured with Celltracker blue-labeled MSCs after drugs were added for 0, 4, 8, 16 and 24h. Immunofluorescence (IF) of Celltracker blue-labeled Ht22 cells and Mitotracker red-labeled MSCs in a coculture system after drugs were added for 1, 2, 3 and 4 days. Drugs including Rsl3 (5 μM), 18-α-GA (50 μM), dynasore (50 μM) or cytochalasin D (200 nM) were used according to different experimental design. Created with BioRender.com. (B) Representative confocal microscopy images of MSC-derived mitochondria (Mitotracker red^{+}) inside Ht22 cells (Celltracker blue^{+}) at 1 day after treated with Rsl3. Scale bar, 20 μm. (C–D) Flow cytometry and quantitative analysis of percentage of Mitotracker green^{+} Ht22 cells (Celltracker blue^{-} Gated) from cocultured with Mitotracker green-labeled MSCs under Rsl3 stimulation for 0, 4, 8, 16 and 24h. (n=3 biological repeats for each group; Ordinary one-way ANOVA). (E–F) Representative scanning electron microscope (SEM) images of tunneling nanotubes (TNTs, red arrow) between neurons and MSCs. In **(E)**, MSC interacts with multiple neurons through short TNTs. In **(F)**, Left: MSC connects with a neuron through a long TNT. Right: magnified view shows the buds (yellow arrow) from the nanotube on the membrane of the MSC. Scale bar, 25 μm (E), 25 μm (F, Left) and 2 μm (F, Right). (G–H) Representative confocal images of TNTs between neurons and MSCs. In **(G)**, a single TNT connects the MSC and the neuron with multiple branches (yellow arrow). Scale bar, 20 μm for original pictures and 5 μm for enlarged pictures. In **(H)**, MIP mode and 3D reconstruction images of Mitotracker localization within F-actin filaments in the TNT. The mitochondria in MSCs were labeled with Mitotracker red. Rhodamine phalloidin 488 was used to label the F-actin filaments in all cells. Scale bar, 1 μm. Two-sided comparison; All data are mean ± SD; Error bars represent SDs; *p < 0.05, ***p < 0.001. See also Supplementary Fig. 4, 5 and 6. (For interpretation of the references to colour in this figure legend, the reader is referred to the Web version of this article.)

Supplementary Figs. 11A–H). Functionally, Cyto D pre-treatment also inhibited the efficacy of MSCs in the improvement of hindlimb behavioral motor functions after SCI, showed by behavioral tests including Basso Mouse Scale (BMS), footprint test and motor evoked potential (MEP) detection (Fig. 7D–H). Besides, the weight loss of mice after SCI regained less by Cyto D pre-treatment as well (Supplementary Fig. 12A). Moreover, at the histological level, disordered lesion area, deposited extracellular matrix and damaged neurons failed to be rescued under Cyto D pre-treatment 42 days after SCI in vivo (Fig. 7I–K and Supplementary Figs. 12B–C), which was consistent with poor neurological function recovery (Fig. 7L and Supplementary Figs. 12D–H).

Altogether, the results indicated that MSC transplantation provoked the restoration of neurological function after SCI, which was blocked by Cyto D pre-treatement. Remarkably, mitochondrial transfer plays an indispensable role in the process, probably by regulating the MQC to inhibit neuronal ferroptosis as shown by the graphical abstract (Fig. 8).

3. Discussion

Intractable as the spinal cord injury (SCI) is, the mechanisms that hinder the neuronal survival and functional rehabilitation is not fully elucidated. In this study, we demonstrated that ferroptosis associated with mitochondrial dysfunction is a critical mechanism of neuronal death after SCI. Targeting mitochondrial quality control (MQC) mechanism could restore mitochondrial homeostasis, alleviate neuronal ferroptosis, and ultimately promote the early recovery of neurological function after SCI. Our work, based on the structural properties and oxidative metabolism of neurons, revealed that SCI is a mitochondria-related disease and that MQC plays a major role in neuronal survival and functional recovery after SCI by alleviating oxidative stress caused by ferroptosis (Fig. 8).

Secondary injury in the acute/subacute phase of SCI can cause programmed neuronal death. It has been pointed out that there are multiple modalities of programmed cell death after SCI. Previous studies on apoptosis of neurons after SCI had few significant outcomes [6], suggesting that there are other ways of programmed cell death leading to neuronal injury. In recent years, more and more studies have focused on non-apoptotic cell death, especially ferroptosis [43]. Ferroptosis leads to intracellular oxidative stress in an iron-dependent manner. In the nervous system, ferroptosis has been shown to be widely involved in the development of diseases, such as neurodegenerative diseases [44], cerebrovascular diseases [9], multiple sclerosis, meningitis [45], traumatic brain injury and SCI [11]. Research on brain revealed that neurons were vulnerable to oxidative stress in a neural identity dependent manner [46]. Furthermore, neurodevelopment analysis has shown that neurons are more sensitive to lipid peroxidation due to its unique lipid component, suggesting that neurons may be more susceptible to ferroptosis [12]. Here, we applied single-cell RNA sequencing analysis to further confirm that neurons are the most vulnerable cell type suffering ferroptosis and that ferroptosis is the main contributor to neuronal death after SCI, which points out a promising target for the rescue of neuronal death.

Mitochondria are the major organelles to produce reactive oxygen species (ROS) and thus lead to the oxidative stress. In addition, mitochondria are widely acknowledged as the key organelles to maintain iron homeostasis [23,24]. Thus, mitochondria can be a powerful target for regulating neuronal ferroptosis to promote the neuronal survival during SCI [47]. The normal function of mitochondria in cells depends on mitochondrial homeostasis, which is maintained predominantly by mitochondrial quality control (MQC). In the process of MQC at the organelle level, damaged mitochondria are dynamically and rapidly neutralized or recycled via balanced fusion, fission and mitophagy to sustain the overall functional health of mitochondria network.

Many studies proved that excessively fragmented mitochondria fail to constitute sufficient mitochondrial respiratory complexes leading to decreased ATP generation and increased ROS accumulation [48,49]. However, the effect of mitophagy on neurons remains controversial. Some studies showed that moderate mitophagy is beneficial to mitochondrial recycling and cellular homeostasis, while others considered that excessive mitophagy aggravates neuronal damage. For example, Zexiang Deng et al. found that the induction of excessive mitophagy in hippocampal neurons caused neuronal damage [50]. In our study, we indicated that excessive mitophagy occurred in neurons during ferroptosis. On the one hand, excessive mitophagy causes mitochondrial dysfunction to generate more ROS. On the other hand, excessive mitophagy leads to the degradation of ferritin in mitochondria and subsequent increase of free iron content in cells so as to provoke the ferroptosis as Fan Yu et al. have demonstrated [51]. In conclusion, our findings raised the possibility that neuronal survival is dependent on the extent of mitochondrial fission and mitophagy and provided new evidence that MQC is involved in the development and progression of CNS diseases.

From the perspective of neuronal activity, sufficient functional mitochondria are indispensably needed to support neuronal viability because neurons are one of the most energy-demanding cells to maintain its normal functions in CNS [52–54]. When damaged neurons with dysfunctional mitochondria fail to compensated themselves rapidly due to disordered MQC, the function and regeneration of axons and synapses are severely affected [30,55]. In recent years, many studies have focused on mitochondrial transfer therapy which directly provides healthy exogenous mitochondria to damaged cells [31,56]. Purified mitochondrial transplantation appears to be practical but it still has many drawbacks [31]. First, studies showed that long-term neuroprotective effect is lacking in the transplantation of isolated mitochondria. Second, it is impossible to supply mitochondria precisely targeting neurons. Third, high concentration of purified mitochondria prone to accumulate and cause extra impairment to neurons. Last but not least, it is difficult to obtain a large number of purified healthy mitochondria and sustain their activity in clinical practice.

In spite of the side effects of purified mitochondrial transplantation

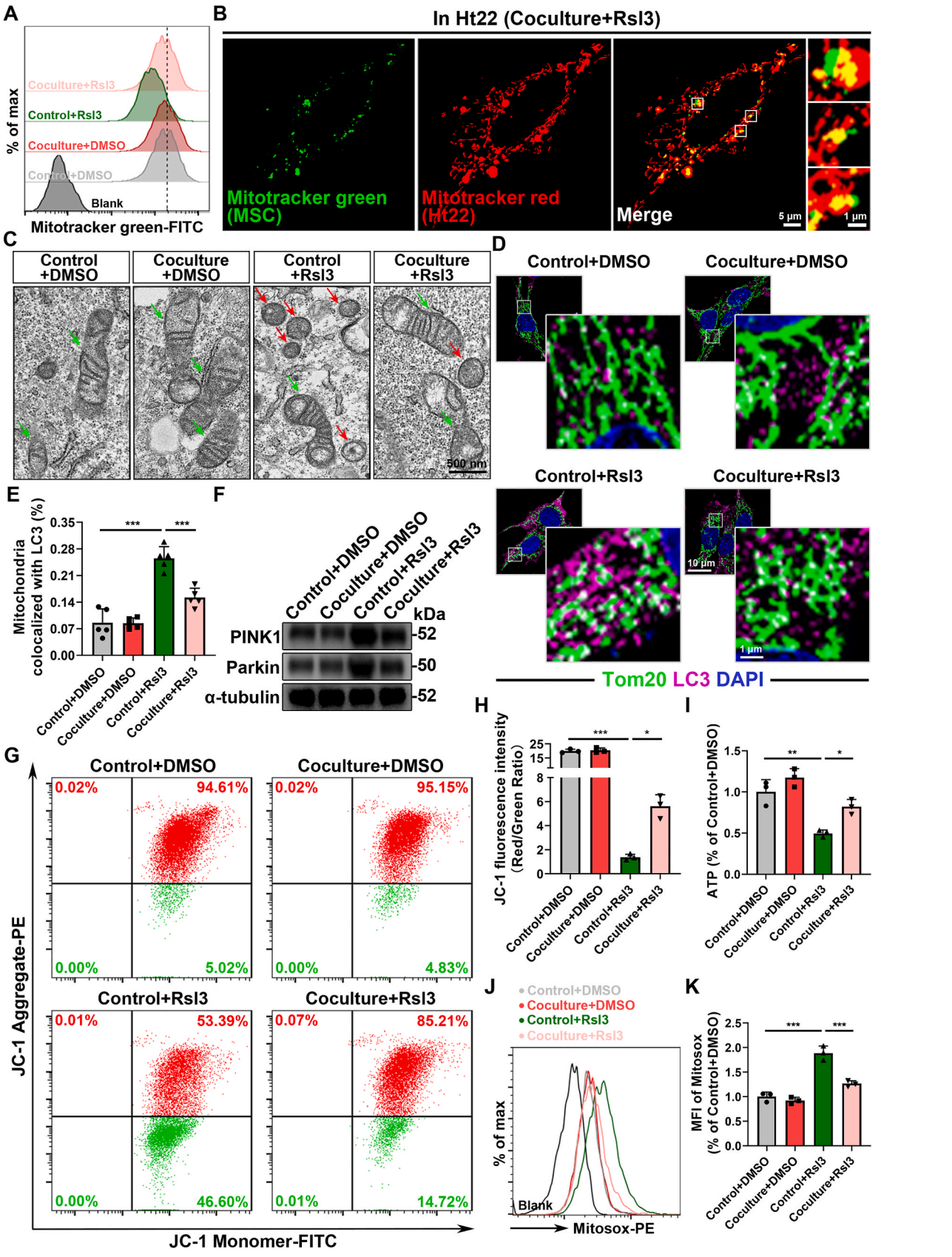

(caption on next page)

Fig. 4. MSC-mediated mitochondrial transfer stabilizes mitochondrial quality control in ferroptotic neurons. (A) Flow cytometry analysis of mitochondrial activity in Ht22 cells from culture alone and coculture with MSCs, treated by DMSO or Rsl3 for 24 h. Mitochondria was stained with Mitotracker green (FITC channel). (B) Representative immunostaining pictures of fused mitochondria (yellow fluorescence) in Ht22 cells coculture with MSCs after Rsl3 stimulation for 24 h. MSCs were labeled with Mitotracker green and Ht22 cells were labeled with Mitotracker red. Scale bar, 5 μm for original pictures and 1 μm for enlarged pictures. (C) Representative transmission electron microscope (TEM) images of mitochondrial morphology in Ht22 cells from culture alone (Control) and coculture with MSCs (Coculture), treated by DMSO or Rsl3 for 24 h. Red and green arrows indicate damaged and normal mitochondria respectively. Scale bar, 500 nm. (D) Representative immunostaining pictures of mitophagy potential in Ht22 cells from culture alone and coculture with MSCs, treated by DMSO or Rsl3 for 24 h. Mitochondria are stained with Tom20 and autophagy is stained with LC3, respectively. Scale bar, 10 μm for original pictures and 1 μm for enlarged pictures. (E) Quantification of the average level of colocalization between mitochondria and LC3 in **(D)**. (n=5 biological repeats for each group; n = 22, 24, 18 and 20 Ht22 cells for Control+DMSO, Coculture+DMSO, Control+Rsl3 and Coculture+Rsl3 group, respectively; Ordinary one-way ANOVA). (F) Western Blot analysis of mitophagy related proteins, such as PINK1 and Parkin, in Ht22 cells from culture alone and coculture with MSCs, treated by DMSO or Rsl3 for 24 h. (G) Flow cytometry analysis of mitochondrial membrane potential (MMP) probed with JC-1 in Ht22 cells from culture alone and coculture with MSCs, treated by DMSO or Rsl3 for 24 h. (H) Quantitative analysis of the ratio of JC-1 aggregates (referred to high MMP, PE channel) /JC-1 monomers (referred to low MMP, FITC channel) in **(G)**. (n=3 biological repeats for each group; Ordinary one-way ANOVA). (I) Measurement of the intracellular ATP level in Ht22 cells from culture alone and coculture with MSCs, treated by DMSO or Rsl3 for 24 h (n=3 biological repeats for each group; Ordinary one-way ANOVA). (J) Flow cytometry analysis of mitochondrial ROS level in Ht22 cells from culture alone and coculture with MSCs, treated by DMSO or Rsl3 for 24 h. Mitochondrial ROS was probed with Mitosox (PE channel). (K) Quantitative analysis of the mean fluorescence intensity of Mitosox in **(J)**. (n=3 biological repeats for each group; Ordinary one-way ANOVA). Two-sided comparison; All data are mean ± SD; Error bars represent SDs; *p < 0.05, **p < 0.01, ***p < 0.001; See also Supplementary Fig. 7. (For interpretation of the references to colour in this figure legend, the reader is referred to the Web version of this article.)

described above, numerous studies have demonstrated the efficacy of intercellular mitochondrial transfer. For example, astrocytes in nerve tissue in situ can deliver mitochondria to alleviate neuronal damage after stroke. However, the neuroprotective effect of astrocytes is short and there has been no available approach for clinical translation by now [57]. In contrast, mesenchymal stem cells (MSCs) which is proved to be effective and safe in tissue repair clinically, can serve as satisfactory donor cells for mitochondrial delivery in clinical treatment [57–59]. In our study, we found that a single MSC could connect with multiple neurons simultaneously to transfer mitochondria via TNTs. These newly identified phenomena indicated that MSC-mediated mitochondrial transfer not only increases the efficacy of transferring mitochondria into neurons by direct intercellular interaction, but also has the capacity of influencing a more extensive range of neurons. From the perspective of mitochondrial regulation in ferroptosis, our study firstly illuminated that neuronal ferroptosis was modulated by the MQC at the cell organelle level. We observed that MSC-derived mitochondria could fuse with damaged neuronal mitochondria to reduce the excessive mitochondrial fission and mitophagy, restored the MQC and eventually inhibited neuronal ferroptosis.

Interestingly, in mice post-SCI, we found that intramedullary MSC injection significantly improved the motor deficits at the early stage (within 7 days), suggesting that MSCs may alleviate neuronal ferroptosis in the acute/subacute phase of SCI through mitochondrial transfer. In addition, given that MSCs have additional anti-inflammatory, paracrine and other multi-dimensional neuroprotective effects apart from mitochondrial transfer itself, MSC-based mitochondrial transfer may have a stronger neuroprotective effect than exogenous mitochondrial transfer alone [60]. In the future, we are expected to provide new ideas for improving the clinical efficacy of MSCs in the treatment of central nervous system diseases by improving the efficiency of the delivery of MSC-derived mitochondria.

However, there are some limitations of our present study about the mitochondrial exchange and MSC transplantation therapy. First, the possibility of reverse direction of mitochondrial transfer from neurons to MSCs is required investigation in detail. Second, the mitochondrial transfer between neurons via tunneling nanotubes was reported to contribute to the repair of neural diseases [61,62]. Therefore, whether the neuron-to-neuron mitochondrial exchange can synergize the beneficial effect of MSC-to-neuron mitochondrial transfer is worth further exploring. Third, apart from the amelioration of neuronal ferroptosis in the acute and (or) subacute phase of SCI shown in our study, prolonged therapeutic effects on neuronal regeneration of MSCs in the chronic phase deserves consideration. Moreover, the time and influencing factors of MSC survival in the SCI microenvironment warrant detailed exploration in the future for guiding the course of MSC therapy in the clinical practice.

In summary, based on the biological characteristics of neural tissue such as highly dependent on mitochondria-dominated oxidative metabolism and poor anti-oxidative stress capacity, we took the lead in finding that neurons are prone to ferroptosis after SCI by single-cell RNA sequencing analysis. Taking the advantages of MSCs to transfer functional mitochondria, we rescued the imbalance of neuronal mitochondrial homeostasis through targeting the MQC, thereby alleviating neuronal ferroptosis, and ultimately promoted the recovery of neurological function after SCI. Our study provides new evidence for revealing that the failure of self-regulation of MQC system is widely involved in the occurrence and development of central nervous system diseases, creatively integrates the mitochondrial therapy and stem cell therapy, and effectively promotes the exploration of the mechanism and clinical treatment of SCI.

4. Methods

4.1. Animals

Animal use and all experiments involving animals were approved by the Ethical Committee of Sun Yat-sen University, China. Only female mice were used throughout the experiment. C57BL/6 mice were purchased from Jiangsu GemPharmatech, which aged 8 weeks. All the animals were provided free access to food and water and kept in a colony room under conditions of constant temperature (25 °C), humidity (70%), and lighting (12 h light/12 h dark cycle) in the Sun Yat-sen University Animal Center.

4.2. Surgeries

4.2.1. Spinal cord injury

The procedure of T10 crush injury of spinal cord was performed according to previous established protocol [63]. In brief, C57BL/6 mice were anesthetized by pentobarbital sodium and a 2 cm midline incision was made over the dorsal thoracic vertebrae, followed by a T9-T10 laminectomy to fully expose the spinal cord. Forceps with a width of 0.1 mm in the last 5 mm of tips were specially used to perform the crush injury (11295–00, F.S.T). Tips of forceps were inserted along bilateral sides of the spinal cord and touched the vertebrae on the ventral side to cover the whole circumference of the spinal cord. The spinal cord was then crushed for 5 s with forceps. Hemorrhagic around the crushed segment could be seen immediately after crushing. The muscle layers were sutured and wound clips were used to close the skin. Mice were placed on a warming blanket after surgery until thoroughly awake and were given buprenorphine and cyclosporin A for pain relief and anti-infection. Dysfunctional bladders were manually emptied once a day until their autonomous urination function recovered.

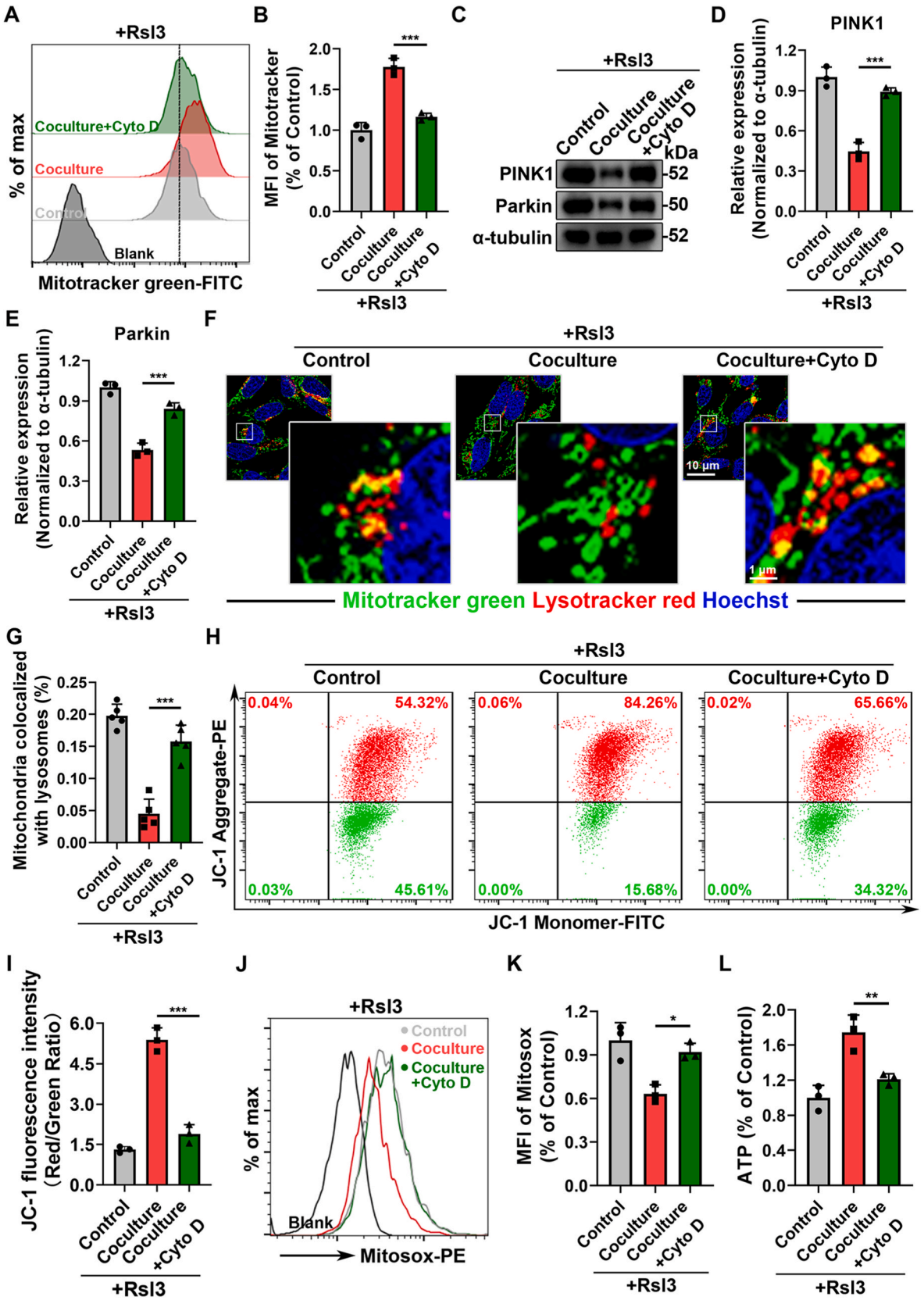

(caption on next page)

Fig. 5. Inhibition of mitochondrial transfer impedes the recovery of mitochondrial quality control mediated by MSCs during neuronal ferroptosis. (A) Flow cytometry analysis of mitochondrial activity in Ht22 cells from culture alone, coculture with MSCs or MSC coculture combined with Cytochalasin D (Cyto D) treatment after Rsl3 stimulation for 24 h. Mitochondria was stained with Mitotracker green (FITC channel). (B) Quantitative analysis of the mean fluorescence intensity of MitoTracker green in **(A)**. (n=3 biological repeats for each group; Ordinary one-way ANOVA). (C) Western Blot analysis of mitophagy related proteins, such as PINK1 and Parkin, in Ht22 cells from culture alone, coculture with MSCs or MSC coculture combined with Cyto D treatment after Rsl3 stimulation for 24 h. (D–E) Quantitative analysis of the expression of mitophagy related proteins in **(C)**. (n=3 biological repeats for each group; Ordinary one-way ANOVA). (F) Representative immunostaining pictures of mitophagy potential in Ht22 cells from culture alone, coculture with MSCs or MSC coculture with Cytochalasin D (Cyto D) treatment after Rsl3 stimulation for 24 h. Mitochondria are stained with Mitotracker green and autophagy is stained with Lysotracker red, respectively. Scale bar, 10 μm for original pictures and 1 μm for enlarged pictures. (G) Quantification of the average level of colocalization between mitochondria and lysosomes in **(F)**. (n=5 biological repeats for each group; Ordinary one-way ANOVA). (H) Flow cytometry analysis of mitochondrial membrane potential (MMP) probed with JC-1 in Ht22 cells from culture alone, coculture with MSCs or MSC coculture combined with Cyto D treatment after Rsl3 stimulation for 24 h. (I) Quantitative analysis of the ratio of JC-1 aggregates (referred to high MMP, PE channel) /JC-1 monomers (referred to low MMP, FITC channel) in **(H)**. (n=3 biological repeats for each group; Ordinary one-way ANOVA). (J) Flow cytometry analysis of mitochondrial ROS level in Ht22 cells from culture alone, coculture with MSCs or MSC coculture combined with Cyto D treatment after Rsl3 stimulation for 24 h. Mitochondrial ROS was probed with Mitosox (PE channel). (K) Quantitative analysis of the mean fluorescence intensity of Mitosox in **(J)**. (n=3 biological repeats for each group; Ordinary one-way ANOVA). (L) Measurement of the intracellular ATP level in Ht22 cells from culture alone, coculture with MSCs or MSC coculture combined with Cyto D treatment after Rsl3 stimulation for 24 h (n=3 biological repeats for each group; Ordinary one-way ANOVA). Two-sided comparison; All data are mean ± SD; Error bars represent SDs; *$p < 0.05$, **$p < 0.01$, ***$p < 0.001$; See also Supplementary Fig. 8. (For interpretation of the references to colour in this figure legend, the reader is referred to the Web version of this article.)

4.2.2. MSC transplantation for SCI mice

Cell transplantation was performed right after the establishment of SCI model according to previous articles [64]. Prior to the crush injury, mice were randomized and assigned to three different groups: SCI group (intramedullary injection of vehicle), SCI+MSC (intramedullary injection of untreated MSC suspension) group, and SCI+MSC+Cyto D group (intramedullary injection of cytochalasin D-pretreated MSC suspension). In the SCI+MSC or SCI+MSC+Cyto D group, 3×10^5 cells were suspended in 2 μL PBS and injected directly into the spinal cord at the crush injury epicenter using a stereotaxic microinjection apparatus (Drill and Injection Robot, Neurostar), 10 μL Hamilton syringe (7653-01, Hamilton) and 33 g removable needle (7803-05, Hamilton). In the SCI group, equal volumes of vehicle were injected in the same manner as that in the MSC suspension intramedullary injection group.

4.3. Cell culture

Ht22 cells (mouse primary hippocampal neurons) were purchased from American Type Culture Collection (ATCC; Rockville, MD, USA) and grown in the high-glucose Dulbecco's Modified Eagle Medium (DMEM; Invitrogen) supplemented with 10% fetal bovine serum (FBS; Invitrogen), 100 IU/mL penicillin (Invitrogen), and 100 μg/mL streptomycin (Invitrogen). Human umbilical MSCs (hUC-MSCs) were gifted from The Biotherapy Center, the Third Affiliated Hospital, Sun Yat-Sen University. MSCs were cultured in the low-glucose DMEM (Invitrogen) supplemented with 10% FBS (Invitrogen), 100 IU/mL penicillin (Invitrogen), and 100 μg/mL streptomycin (Invitrogen). All the cells were cultured in a humidified 5% CO_2 - 95% air environment at 37 °C.

For in vitro drug treatment experiments, RAS-selective-lethal-3 (Rsl3, CSN17581, CSNpharm) is a classical ferroptosis inducer [7,42]. 5 μM Rsl3 was used to induce intracellular ferroptosis in Ht22 cells. 18-α-GA, dynasore, and cytochalasin D (Cyto D) were purchased from Sigma-Aldrich and were used in a concentration of 50 μM, 50 μM, and 200 nM, respectively.

For fluorescence staining of cell, mitochondria and lysosome, 20 μM Celltracker blue CMF2HC Dye (C12881, Invitrogen), 500 nM Mitotracker green FM (9074S, Cell Signaling Technology), 500 nM Mitotracker red CMXRos (9082S, Cell Signaling Technology) and 1 μM Lysotracker red DND-99 (L7528, Invitrogen) was used according to the manufacturers' protocols respectively. Ht22 cells or MSCs were incubated with indicated fluorescent dyes in culture media and the excess dye was washed out by PBS. Then, after 2 days, stained cells were seeded for monoculture and coculture.

4.4. hUC-MSCs characterization

For phenotypic characterization, hUC-MSCs were identified as previously described [65]: (1) plastic adhesion growth; (2) expression of surface markers: more than 95% of the cells expressed CD105, CD73, and CD90, while less than 2% of the cells expressed CD45, CD34, CD11b, CD19, and HLA-DR; and (3) potential of trilineage differentiation into osteoblasts, adipocytes, and chondroblasts in vitro. As shown in Supplementary Fig. 4, the isolated hUC-MSCs met the identification standards, and the well-characterized 5th–7th passage hUC-MSCs were used for both in vivo and in vitro experiments.

4.5. In vitro differentiation of hUC-MSCs

4.5.1. Osteogenic differentiation

For osteogenic differentiation potential determination, hUC-MSCs were cultured in α-MEM (Invitrogen), 10% FBS (Invitrogen), 50 μg/ml ascorbic acid (Sigma), 10 mM β-glycerophosphate (Sigma), 10 nM dexamethasone (Sigma), 100 U/ml streptomycin (Invitrogen), and 100 U/ml penicillin (Invitrogen) for 2 weeks and the induction medium was changed every 3 days. The osteogenic-differentiated cells were fixed and stained with Alizarin red S (Sigma) for calcium detection, as previously described [66].

4.5.2. Adipogenic differentiation

For adipogenic differentiation potential determination, hUC-MSCs were cultured in induction medium A consisting of high-glucose DMEM (Invitrogen), 10% FBS (Invitrogen), 0.5 mM 3-isobutyl-1-methylxanthine (Sigma), 10 μg/ml insulin (Sigma), 100 nM dexamethasone (Sigma), 0.2 mM indomethacin (Sigma), 100 U/ml streptomycin (Invitrogen), and 100 U/ml penicillin (Invitrogen) for 3 days, followed by culture of maintenance medium consisting of high-glucose DMEM (Invitrogen), 10% FBS (Invitrogen), 10 μg/ml insulin (Sigma), 100 U/ml streptomycin (Invitrogen), and 100 U/ml penicillin (Invitrogen) for 1 day, together as a cycle. After 3 cycles of culture, cells were cultured in maintenance medium for another 7 days. The adipogenic-differentiated cells were confirmed by Oil red O (Sigma) staining, as previously described [66].

4.5.3. Chondrogenic differentiation

For chondrogenic differentiation potential determination, hUC-MSCs were induced using a cell pellet culture system as previous described [67]. Briefly, hUC-MSCs were suspended in 15 ml conical tube containing 2 ml induction medium of high-glucose DMEM (Invitrogen), 3% FBS (Invitrogen), 10 ng/ml TGFβ3 (Pepro Tech), 1x ITS (Sigma) and 1 mM pyruvate (Sigma) for 4 weeks and the induction medium was changed every 3 days. The chondrocytes were identified by toluidine blue (Sigma) staining, as previously described [66].

4.6. Coculture assay

For the contact coculture, Ht22 cells and MSCs were cocultured at a 1:1 ratio in the high-glucose DMEM (Invitrogen) supplemented with 10% FBS (Invitrogen), 100 IU/mL penicillin (Invitrogen), and 100 μg/mL streptomycin (Invitrogen). After 12 h of coculture, the medium was replaced into fresh one, and treated with or without drugs as described above. Mono-cultured Ht22 cells served as a control. After indicated

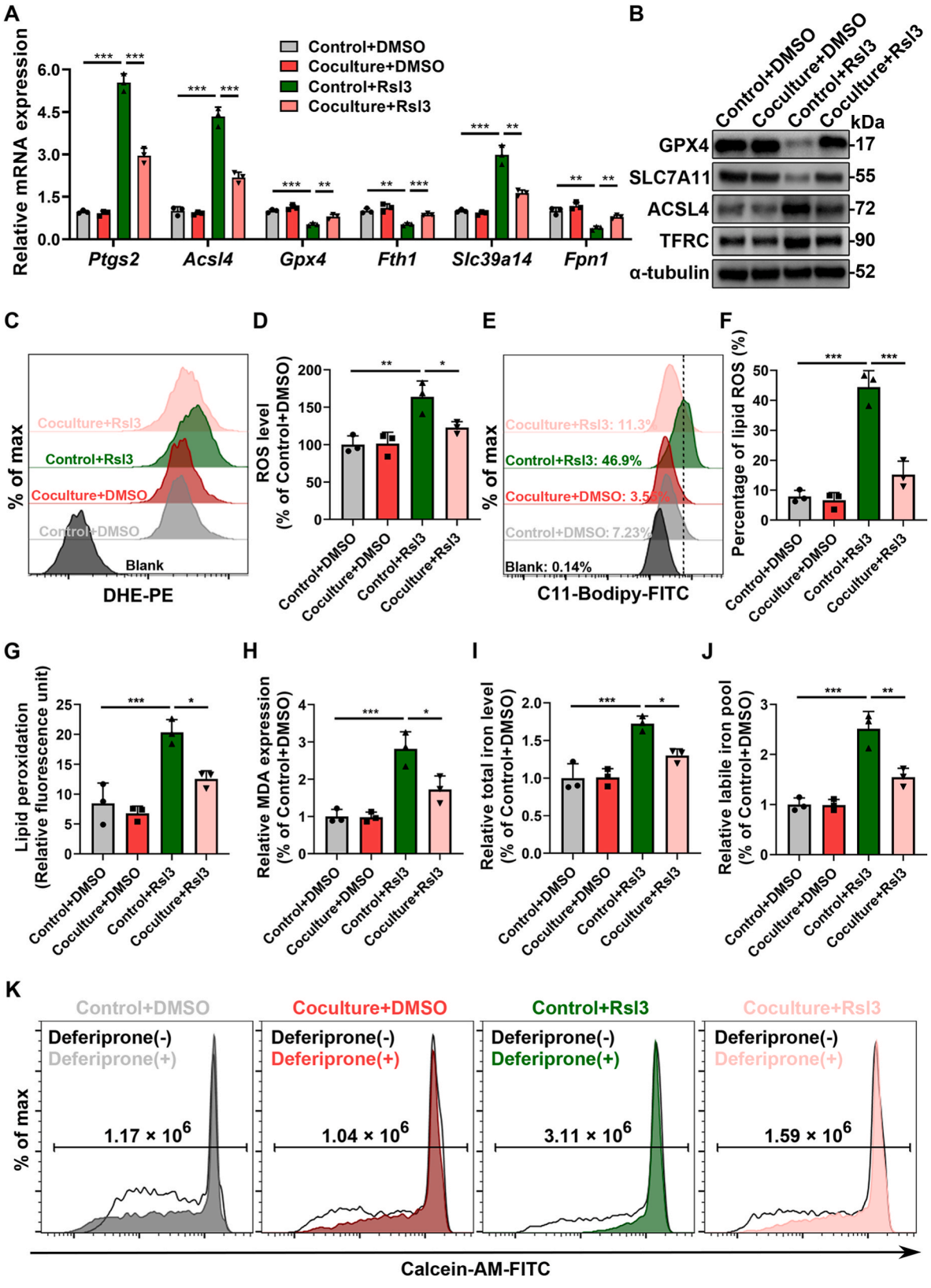

(caption on next page)

Fig. 6. MSC coculture inhibits neuronal ferroptosis through mitochondrial transfer. (A) qPCR analysis of relative mRNA expression of ferroptosis-related genes, including *Ptgs2*, *Acsl4*, *Gpx4*, *Fth1*, *Slc39a14* and *Fpn1*, in Ht22 cells from culture alone, coculture with MSCs or MSC coculture combined with Cyto D treatment after Rsl3 stimulation for 24 h (n=3 biological repeats for each group; Ordinary one-way ANOVA). (B) Western Blot analysis of the ferroptosis-related proteins in Ht22 cells from culture alone, coculture with MSCs or MSC coculture combined with Cyto D treatment after Rsl3 stimulation for 24 h (n=3 biological repeats for each group). (C–D) Flow cytometry and quantitative analysis of intracellular ROS level in Ht22 cells from culture alone, coculture with MSCs or MSC coculture combined with Cyto D treatment after Rsl3 stimulation for 24 h. Intracellular ROS was stained with DHE (PE channel). (n=3 biological repeats for each group; Ordinary one-way ANOVA). (E) Flow cytometry analysis of intracellular lipid ROS generation in Ht22 cells from culture alone, coculture with MSCs or MSC coculture combined with Cyto D treatment after Rsl3 stimulation for 24 h. Intracellular lipid ROS was probed with C11-BODIPY$^{581/591}$ (oxidized, FITC channel). (F) Quantitative analysis of the percentage of oxidized C11-BODIPY$^{581/591}$ in **(E)**. (n=3 biological repeats for each group; Ordinary one-way ANOVA). (G) Quantitative analysis of the ratio of oxidized (FITC channel) to reduced (PE channel) C11-BODIPY$^{581/591}$ mean fluorescence intensity (MFI) in **(E)**. (n=3 biological repeats for each group; Ordinary one-way ANOVA). (H) Measurement of intracellular MDA level in Ht22 cells from culture alone, coculture with MSCs or MSC coculture combined with Cyto D treatment after Rsl3 stimulation for 24 h (n=3 biological repeats for each group; Ordinary one-way ANOVA). (I) Measurement of intracellular total iron level in Ht22 cells from culture alone, coculture with MSCs or MSC coculture combined with Cyto D treatment after Rsl3 stimulation for 24 h (n=3 biological repeats for each group; Ordinary one-way ANOVA). (J) Quantitative analysis of the increase in MFI of Calcein-AM (FITC channel, subtracted the MFI treated without Deferiprone from the MFI treated with Deferiprone), reflected the amount of intracellular labile iron pool (LIP) in **(K)**. (n=3 biological repeats for each group; Ordinary one-way ANOVA). (K) Flow cytometry analysis of LIP in Ht22 cells from culture alone, coculture with MSCs or MSC coculture combined with Cyto D treatment after Rsl3 stimulation for 24 h. Cells were incubated by Calcein-AM (FITC channel) and treated with or without Deferiprone. Two-sided comparison; All data are mean ± SD; Error bars represent SDs; *p < 0.05, **p < 0.01, ***p < 0.001; See also Supplementary Fig. 9 and Fig. 10.

time of coculture, the cells were harvested for indicated experiments.

4.7. Mito-GFP Lentivirus transfection

Lentivirus containing Mito-GFP recombinant gene was purchased from Shanghai Genechem Co., Ltd. Briefly, cells were transfected with the Mito-GFP Lentivirus according to the manufacturer's instruction. After 3 days, green fluorescence of mitochondria in cells was visible under fluorescent microscope, indicating the effective transfection. GFP-labeled MSCs were purified by FACS (BD influx).

4.8. RNA isolation and real-time quantitative PCR

Total RNA was extracted from cells using the RNAzol RT (Molecular Research Center, Inc.) and complementary DNA (cDNA) was synthesized using a RevertAid First Strand cDNA Synthesis Kit (K1622, Thermo Fisher Scientific) according to the manufacturers' protocols. In brief, concentration of total RNA was quantified with a NanoDrop 8000 spectrophotometer and 1 μg of total RNA was used for reverse transcription. Target mRNA levels were quantified by performing qRT-PCR with a FastStart Essential DNA Green Master Mix (06924204001, Roche), as described by the manufacturers' protocols. The thermocycling protocol for all experiments was 40 cycles of denaturation at 95 °C for 10 s, annealing at 60 °C for 10 s, and extension at 72 °C for 30 s. All samples were run in triplicate and target mRNA levels were normalized to those of 18S. The primers designed and used for qPCR are described in Supplementary Table 1.

4.9. Western Blot

Cell suspensions were collected and washed three times with cold phosphate-buffered saline. Then, the cells were lysed in 1X RIPA buffer with 1X protein inhibitor solution for at least 30 min, and centrifuged at 10,000 g for 10 min at 4 °C to remove cell debris. The protein supernatant was aspirated and mixed with 4X loading buffer (Bio-RED). After total protein concentration was measured using BCA Protein Assay Kit (Thermo Scientific), equal amounts of total proteins were resolved by 10% SDS-PAGE (Bio-Rad) and then electrotransferred to a 0.2 μm pore-sized polyvinylidene difluoride membrane (Millipore, Darmstadt). After blocked with 5% BSA, the membrane was incubated with the primary antibodies at 4 °C overnight, followed by incubation with HRP-conjugated secondary antibodies for 1 h at room temperature. The primary and secondary antibodies used can be found in Supplementary Table 1. The chemiluminescent substrate (Millipore) was used to detect the signal intensity. Bands from at least three independent blots were quantified using the Image J software.

4.10. Flow cytometry

Flow cytometric analysis was performed with CytoFLEX (Beckman Coulter) flow cytometers. Data were analyzed with FlowJo v10.6.2 software. The fluorescent markers used for flow cytometry are described in Supplementary Table 1.

4.11. Immunocytochemistry and immunofluorescence

Cells were seeded onto coverslips and treated accordingly for each experiment. If necessary, fixation of cells occurred in 4% paraformaldehyde (PFA) for 15 min. Subsequently, cells were incubated with fluorescent dyes according to manufacturer's instructions. The fluorescent dyes applied were listed in Supplementary Table 1. Images were taken using an LSM880 confocal microscope with Airyscan (Zeiss). Live-cell imaging was performed using a commercial structured illumination microscope (HIS-SIM) by following the previous report [68].

Spinal cord samples were fixed in 4% PFA and then embedded in OCT compound for subsequent sectioning. Each tissue section was incubated with the primary antibodies overnight at 4 °C, followed by incubation with secondary antibodies away from light for 1 h at room temperature. The primary and secondary antibodies used were described in Supplementary Table 1. Images were acquired using LSM800 confocal microscope (Zeiss) or Dragonfly CR-DFLY-202 2540 (Leica).

4.12. Histological analysis

H&E, Nissl and Masson staining were carried out for histological analysis. After sacrifice, mouse T10 spinal cord segment that involves the injury epicenter was dissected, perfused with 4% PFA and prepared for the paraffin embedding. The paraffin-embedded spinal cord segment was sectioned longitudinally into 4 μm thick slices. The paraffin sections were deparaffinized and rehygrated in PBS. Hematoxylin and eosin (H&E) and cresyl violet were used for the H&E and Nissl staining respectively. Masson' s trichrome staining was performed for the detection of collagen deposition. The sections were analyzed, and images were captured using an AxioScan. Z1 microscope (Zeiss).

4.13. Transmission electron microscopy

Cell samples were fixed in 2.5% glutaraldehyde for 2 h at room temperature and then stored at 4 °C overnight. Subsequently, samples were post-fixed with 1% osmium tetroxide for 1 h, washed, dehydrated through an ethanol gradient (30, 50, 70 and 95%, 5 min per step), embedded and polymerized at 60 °C for 48 h. Ultrathin sections of 85 nm were cut and observed in a Tecnai 12 BioTwin transmission electron

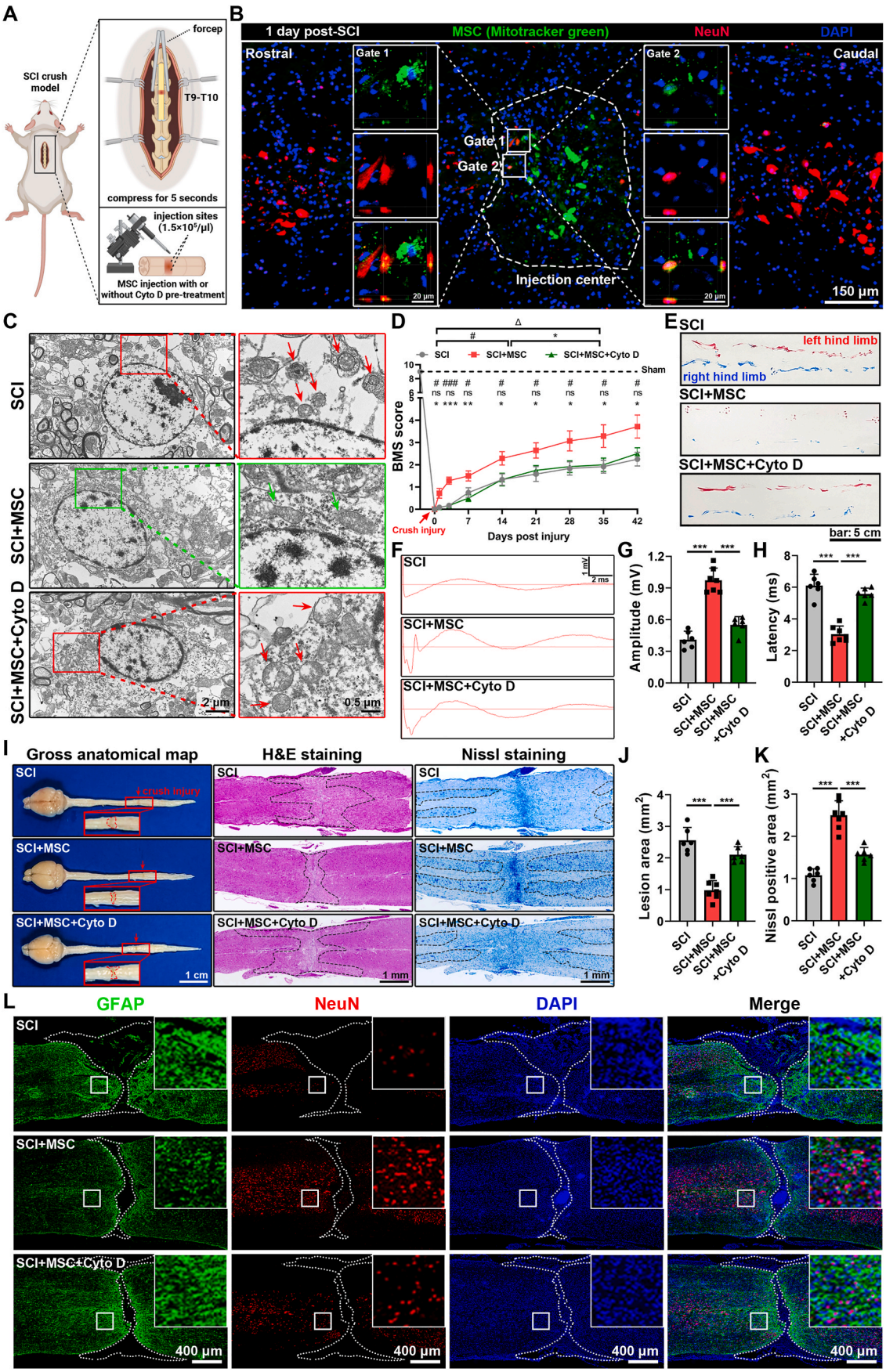

(caption on next page)

Fig. 7. MSC transplantation alleviates neuronal ferroptosis and promotes functional recovery after SCI by delivery of mitochondria. (A) Schematic illustration of spinal crush injury model and MSC intramedullary injection post injury. Created with BioRender.com. (B) Representative confocal microscopy images show rostal part, injection center and caudal part of spinal cord tissues in 1 day after spinal cord injury. Mitochondriaderived from MSCs were labeled by Mitotracker and neurons were marked by NeuN. Scale bar, 150 μm for original pictures and 20 μm for enlarged pictures. (C) Representative TEM images show the morphology of neuronal mitochondria in the spinal cord tissue from SCI group, SCI+MSC group, SCI+MSC+Cyto D group in 1 day after spinal cord injury. Red and green arrows indicate damaged and normal mitochondria, respectively. Scale bar, 2 μm for original pictures and 0.5 μm for enlarged pictures. (D) Measurement of BMS scores on day 0, 1, 3, 7, 14, 21, 28, 35 and 42 post injury. (n=6 biological repeats for SCI group, SCI+MSC+Cyto D group and n=7 biological repeats for SCI+MSC group; Ordinary one-way ANOVA). (E) Representative images of footprint test in 42 days after spinal cord injury from SCI group, SCI+MSC group, SCI+MSC+Cyto D group. Scale bar, 5 cm. (F) Representative diagrams of motor evoked potential (MEP) detection in 42 days after spinal cord injury from SCI group, SCI+MSC group, SCI+MSC+Cyto D group. (G–H) Quantitative analysis of the amplitude of the first peak (mV) and the latency (ms) in **(F)**. (n=6 biological repeats for SCI group, SCI+MSC+Cyto D group and n=7 biological repeats for SCI+MSC group; Ordinary one-way ANOVA). (I) Representative gross anatomical maps, H&E and Nissl staining images show the lesion core and neuronal region in 42 days after spinal cord injury from SCI group, SCI+MSC group, SCI+MSC+Cyto D group, respectively. Scale bar, 1 cm for gross anatomical maps and 1 mm for staining images. (J–K) Quantitative analysis of the lesion area and Nissl staining positive area (mm^2) in **(I)**. (n=6 biological repeats for SCI group, SCI+MSC+Cyto D group and n=7 biological repeats for SCI+MSC group; Ordinary one-way ANOVA). (L) Representative immunostaining pictures of the spinal cord in 42 days after spinal cord injury from SCI group, SCI+MSC group, SCI+MSC+Cyto D group, Neurons were marked by NeuN and astrocytes were marked by GFAP to indicate the lesion area. Scale bar, 400 μm. Two-sided comparison; All data are mean ± SD; Error bars represent SDs; *p < 0.05, **p < 0.01, ***p < 0.001, ns > 0.05; See also Supplementary Figs. 11 and 12. (For interpretation of the references to colour in this figure legend, the reader is referred to the Web version of this article.)

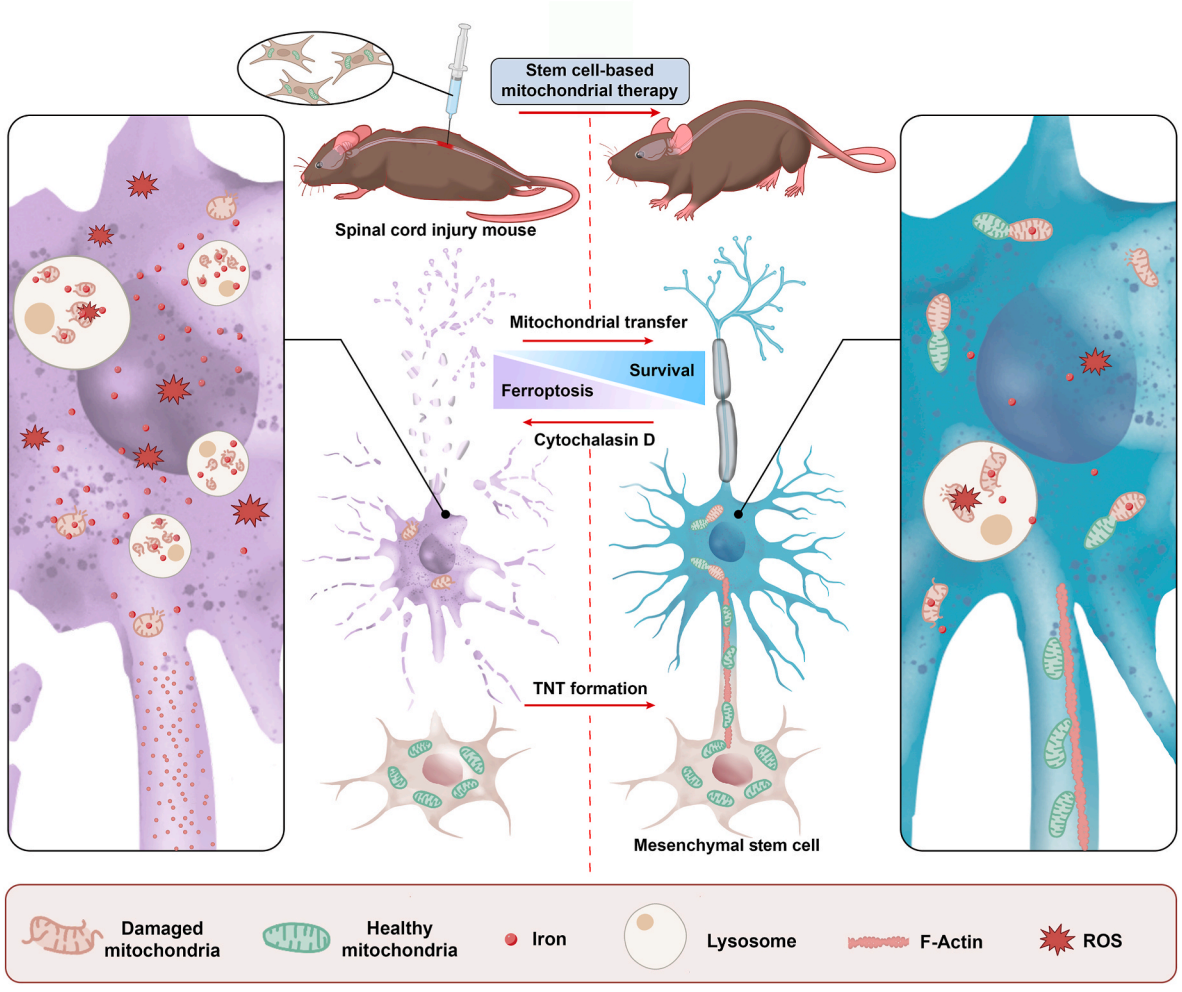

Fig. 8. Schematic illustration of stem cell-based mitochondrial therapy **for anti-neuronal ferroptosis** during spinal cord injury. Injection of abundant functional mitochondria based on mesenchymal stem cell (MSC) in vivo stabilizes neuronal mitochondrial quality control system, alleviates neuronal ferroptosis and finally promotes functional recovery after spinal cord injury. Pharmacological intervention by cytochalasin D reduces by tunneling nanotube (TNT)-dependent mitochondrial transfer, increasing neuronal ferroptosis and decreasing the effect of stem cell-based mitochondrial therapy for spinal cord injury.

microscope (FEI Company, Eindhoven, The Netherlands) at 120 keV.

For tissue microscopy, the T10 segment of spinal cord was isolated and sliced in 1 mm thick longitudinal sections. The fixed tissues were embedded using EPON as previously descried. Ultrathin sections of 70 nm were cut using an ultramicrotome (Leica Microsystems, UC6) with a diamond knife (Diatome, Biel, Switzerland) and stained with 1.5% uranyl acetate at 37 °C for 15 min and lead citrate solution for 4 min. Electron micrographs were taken with a JEM-2100 Plus Transmission Electron Microscope (JEOL), equipped with Camera OneView 4 K 16 bit (Gatan) and software Digital Micrograph (Gatan).

For analysis, the length and morphology of each mitochondrion was determined in ImageJ following manual drawing of single organelle. All

parameters obtained from one field of view were averaged together.

4.14. Scanning electron microscopy

The intercellular tunneling nanotubes between Ht22 cells and MSCs were visualized by scanning electron microscopy. In brief, Ht22 cells and MSCs were cocultured on 15 mm diameter glass coverslips for the desired time. Cells were fixed 2.5% glutaraldehyde overnight. After fixation, the samples were washed with PBS before dehydration using an ethanol gradient, followed by replacement of ethanol with acetone and isoamyl acetate. After fixation and dehydration, the samples were critical point-dried using (EM, CPD300, Leica) and coated with gold using (MC1000, Hitachi). lmages were done using an FEI Quanta 200 scanning electron microscope.

4.15. Basso mouse scale (BMS) score

Locomotor function of mice was evaluated using an open-field score, the BMS as previously reported [69]. Briefly, on the 0, 1st, 3rd, 7th, 14th, 21st, 28th, 35th, 42th days after injury, all mice were allowed to crawl freely and evaluated by two independent researchers who were blind to the treatment groups. The score was based on the ankle movement, plantar placing, plantar stepping and motor coordination.

4.16. Footprint test

Footprint test was used to observe the gait recovery and motor coordination according to established previous article [70]. Briefly, on the 42th day after SCI injury, mice were encouraged to crawl along a straight line on a piece of white paper three times with their left and right hind paws painted by blue and red dye, respectively. Footprint traces were printed on the paper and digitized by the camera.

4.17. Motor evoked potential (MEP) detection

The function of motor nervous system of lower limbs was tested by MEP detection on the 42th day after the SCI injury. BL-420A/F Data Acquisition Analysis System (TECHMAN SOFT) was applied. The motor cortex of mice was exposed and touched by stimulating electrodes. The recording electrodes were placed on the contralateral sciatic nerve. The latency and amplitude of the first evoked peak were selected as parameters for assessment of the function of the motor neuron.

4.18. Measurements of intracellular total iron

The level of intracellular total iron (Fe^{2+} and Fe^{3+}) was determined using Intracellular Iron Colorimetric Assay Kit (E1042, APPLYGEN) according to the instruction. After processed with working solution at 60 °C for 15 min, cell lysate and standard sample were incubated with iron probe at 37 °C for 30 min. The absorbance at 550 nm was measured by the microplate reader (Sunrise, TECAN). Concentrations of intracellular total iron were calculated according to standard curve. Protein concentrations of each sample should be determined for the measurement of intracellular total iron per unit of protein.

4.19. Measurements of labile iron pool (LIP)

The level of labile iron pool was measured by calcein-acetoxymethyl ester (Calcein-AM, GC34061, GLPBIO) cooperated with deferiprone (HY–B0568, MCE). After trypsinization, cells (6-well dishes) were washed twice with PBS and then incubated with 1 μM Calcein-AM at 37 °C for 15 min. Subsequently, cells were washed twice with PBS followed by incubation with or without 1 μM deferiprone at 37 °C for 1 h. Following rinsing with PBS, cells were analyzed by flow cytometry. Calcein-AM was excited at 488 nm, and fluorescence was measured at 525 nm. The difference in the mean fluorescence intensity (MFI) of cells with and without deferiprone incubation reflected the amount of the LIP.

4.20. Measurements of ROS, lipid ROS and MDA

Intracellular ROS levels were determined by DHE Assay Kit (ab236206, Abcam) according to the manufacturer's instruction. Briefly, cells were incubated in DMEM containing 10 μmol/L DHE at 37 °C for 30 min at dark. After washing, labeled cells were evaluated by flow cytometry. Data were expressed as the MFI and analyzed by FlowJo v10.6.2 software.

Lipid-ROS levels within cells were determined as previously described [71]. In brief, Cells were incubated with fluorescent C11-Bodipy (1 μM; Invitrogen) at 37 °C for 30 min before harvested by trypsin. The cell suspension was subsequently assessed by flow cytometer (Beckman Coulter) using the 488 nm laser for excitation. The signals from both the oxidized C11-Bodipy (FITC channel) and non-oxidized C11 Bodipy (PE channel) were collected. The MFI of both oxidized and non-oxidized C11-Bodipy was calculated for each sample. Data were expressed as the fraction of oxidized C11-Bodipy and conducted by FlowJo v10.6.2 software.

MDA was used for the evaluation of oxidative stress. MDA assay kit (S0131S, Beyotime) was applied to this measurement and the procedures followed the manufacturer's protocol. The protein extraction of cell samples and standard solution of MDA were prepared and respectively incubated with MDA working solutions at 100 °C for 15 min, followed by centrifugation at 1000*g* for 10 min. The absorbance of the supernatant at 532 nm was measured by the microplate reader (Sunrise, TECAN), representing the relative concentration of protein extraction.

4.21. Measurements of mitochondrial ROS

Mitochondrial ROS levels were detected using the fluorescent dye MitoSOX™ Red (M36008, Invitrogen). Cells were incubated in the medium with MitoSOX™ Red for 30 min according to the manufacturer' s protocol. After washing, labeled cells were evaluated using flow cytometry. Data were analyzed by FlowJo v10.6.2 software.

4.22. Mitochondrial activity assay

The mitochondrial activity was determined by the Mitotracker as previously described [72]. In brief, cells were incubated with 500 nM Mitotracker Green FM (9074S, Cell Signaling Technology). The Mitotracker fluorescence was determined by FITC channel by flow cytometry.

4.23. Measurement of mitochondrial membrane potential (MMP)

MMP was measured using an enhanced mitochondrial membrane potential assay kit with JC-1 (C2003S, Beyotime Biotechnology). In brief, cells were incubated with JC-1 staining solution at 37 °C for 20 min, washed with JC-1 staining buffer, and immersed in the medium. Normal mitochondria with JC-1 aggregates produced red fluorescence, and depolarized mitochondria with JC-1 monomers produced green fluorescence. Fluorescent intensity was quantified by flow cytometry. Data were analyzed with FlowJo v10.6.2 software and $\Delta\Psi m$ was expressed as the ratio of red to green fluorescence intensity.

4.24. Measurement of ATP content

Intracellular ATP production was measured using a CellTiter-Glo Luminescent Cell Viability Assay kit (S0026B, Beyotime Biotechnology) as the manufacturer's instructions. Briefly, cells were plated in a 96-well plate, mixed with an equal volume of reagent for 2 min, and incubated at room temperature for 10 min. Luminescence was recorded using a GENios Plus fluorescence microplate reader (Sunrise, TECAN).

4.25. scRNA-seq data processing

The single-cell RNA sequencing data of mouse spinal cord was download from figshare with the identifier (https://doi.org/10.6084/m9.figshare.17702045) [33]. Seurat (version 4.1.3) was used to perform the data procession. After quality control, normalization, cell clustering and cell type annotation, we performed the following analyses: compositional analysis, differential expression testing, gene set variation, and gene set enrichment.

4.26. Statistics and reproducibility

All experiments were carried out with at least three biological replicates and successful reproducibility were shown. All data are reported as the mean ± standard deviation (SD) of at least three independent experiments. Sample sizes are all presented in the figure legends. Statistical analysis between two groups was performed using unpaired *t*-test. Statistical analysis between multiple groups was performed by one-way ANOVA or Tukey's multiple comparison test. All data were analyzed using GraphPad Software. A two-sided p-value < 0.05 was considered to be statistically significant. The level of significance defined as $p < 0.05$ (*), $p < 0.01$ (**), $p < 0.001$ (***).

Data availability statement

Authors declare that data supporting the findings of this study are available within the article and its Supplementary information files or from the corresponding author (S.A.S.) upon request. All uncropped western blots and data values for all figures are provided in the source data file. Source data are provided with this paper.

Code availability

All software and bioinformatic tools used in the present study are publicly available.

Support statement

National Natural Science Foundation of China (82102642, U22A20297, 82172433, 82072455, 81971372, 32170799, 82372400); Guangdong Basic and Applied Basic Research Foundation (2023A1515010313, 2023B1515020016); Special Project for Research and Development in Key Areas of Guangdong Province (2019B020236002); Shenzhen Science Technology and Innovation Commission (JCYJ20210324120804013); Guangzhou Science and Technology Program key projects (202206060003, 202102080212).

Fundamental Research Funds for the Central Universities, Sun Yat-sen University (23ykbj003)

Author contributions

Conceptualization, L.R., P.X., J.W. and S.Y.; Methodology, B.L., S.Y., Y.W., Y.L., Y.L. and Z.X.; Investigation, S.Y., M.P., Y.W., X.W., J.H., C.D. and Y.Q.; Formal Analysis, S.Y., M.P., Y.W., X.W. and Y.G.; Writing, S.Y., M.P. and Y.W.; Funding Acquisition, L.R., P.X., J.W., B.L. and M.P.; Supervision, L.R., P.X. and S.Y.

Declaration of competing interest

The authors declare that they have no known competing financial interests or personal relationships that could have appeared to influence the work reported in this paper.

Acknowledgements

We thank the Core Facility of Center, Zhongshan School of Medicine, Sun Yat-Sen University for providing instruments for a Zeiss 800 Laser Scanning Confocal Microscope, a Zeiss 880 Laser Scanning Confocal Microscope with Airyscan and also thank Guangzhou CSR Biotech Co. Ltd for live-cell imaging by using their commercial super-resolution microscope (HIS-SIM), data acquisition, SR image reconstruction, analysis and discussion.

Appendix A. Supplementary data

Supplementary data to this article can be found online at https://doi.org/10.1016/j.redox.2023.102871.

References

[1] J.W. McDonald, C. Sadowsky, Spinal-cord injury, Lancet 359 (2002) 417–425, https://doi.org/10.1016/S0140-6736(02)07603-1.
[2] J. Guest, N. Datta, G. Jimsheleishvili, D.R. Gater Jr., Pathophysiology, classification and comorbidities after traumatic spinal cord injury, J. Personalized Med. 12 (2022), https://doi.org/10.3390/jpm12071126.
[3] M.V. Sofroniew, Dissecting spinal cord regeneration, Nature 557 (2018) 343–350, https://doi.org/10.1038/s41586-018-0068-4.
[4] A.P. Tran, P.M. Warren, J. Silver, The biology of regeneration failure and success after spinal cord injury, Physiol. Rev. 98 (2018) 881–917, https://doi.org/10.1152/physrev.00017.2017.
[5] A. Alizadeh, S.M. Dyck, S. Karimi-Abdolrezaee, Traumatic spinal cord injury: an overview of pathophysiology, models and acute injury mechanisms, Front. Neurol. 10 (2019) 282, https://doi.org/10.3389/fneur.2019.00282.
[6] A. Anjum, et al., Spinal cord injury: pathophysiology, multimolecular interactions, and underlying recovery mechanisms, Int. J. Mol. Sci. 21 (2020), https://doi.org/10.3390/ijms21207533.
[7] S.J. Dixon, et al., Ferroptosis: an iron-dependent form of nonapoptotic cell death, Cell 149 (2012) 1060–1072, https://doi.org/10.1016/j.cell.2012.03.042.
[8] A. Ashraf, J. Jeandriens, H.G. Parkes, P.W. So, Iron dyshomeostasis, lipid peroxidation and perturbed expression of cystine/glutamate antiporter in Alzheimer's disease: evidence of ferroptosis, Redox Biol. 32 (2020) 101494, https://doi.org/10.1016/j.redox.2020.101494.
[9] I. Alim, et al., Selenium drives a transcriptional adaptive Program to block ferroptosis and treat stroke, Cell 177 (2019) 1262–1279, https://doi.org/10.1016/j.cell.2019.03.032, e1225.
[10] B. Do Van, et al., Ferroptosis, a newly characterized form of cell death in Parkinson's disease that is regulated by PKC, Neurobiol. Dis. 94 (2016) 169–178, https://doi.org/10.1016/j.nbd.2016.05.011.
[11] Q.S. Li, Y.J. Jia, Ferroptosis: a critical player and potential therapeutic target in traumatic brain injury and spinal cord injury, Neural Regen Res 18 (2023) 506–512, https://doi.org/10.4103/1673-5374.350187.
[12] Y. Zou, et al., Plasticity of ether lipids promotes ferroptosis susceptibility and evasion, Nature 585 (2020) 603–608, https://doi.org/10.1038/s41586-020-2732-8.
[13] Z. Geng, et al., Ferroptosis and traumatic brain injury, Brain Res. Bull. 172 (2021) 212–219, https://doi.org/10.1016/j.brainresbull.2021.04.023.
[14] H.I. Ingolfsson, et al., Computational lipidomics of the neuronal plasma membrane, Biophys. J. 113 (2017) 2271–2280, https://doi.org/10.1016/j.bpj.2017.10.017.
[15] Y. Kang, et al., Identification of ferroptotic genes in spinal cord injury at different time points: bioinformatics and experimental validation, Mol. Neurobiol. 59 (2022) 5766–5784, https://doi.org/10.1007/s12035-022-02935-y.
[16] X. Hu, et al., Progress in understanding ferroptosis and its targeting for therapeutic benefits in traumatic brain and spinal cord injuries, Front. Cell Dev. Biol. 9 (2021) 705786, https://doi.org/10.3389/fcell.2021.705786.
[17] Z. Shi, et al., Programmed cell death in spinal cord injury pathogenesis and therapy, Cell Prolif. 54 (2021), e12992, https://doi.org/10.1111/cpr.12992.
[18] H. Ge, et al., Ferrostatin-1 alleviates white matter injury via decreasing ferroptosis following spinal cord injury, Mol. Neurobiol. 59 (2022) 161–176, https://doi.org/10.1007/s12035-021-02571-y.
[19] J. Cheng, et al., Carnosic acid protects against ferroptosis in PC12 cells exposed to erastin through activation of Nrf2 pathway, Life Sci. 266 (2021) 118905, https://doi.org/10.1016/j.lfs.2020.118905.
[20] M.H. Ge, et al., Zinc attenuates ferroptosis and promotes functional recovery in contusion spinal cord injury by activating Nrf2/GPX4 defense pathway, CNS Neurosci. Ther. 27 (2021) 1023–1040, https://doi.org/10.1111/cns.13657.
[21] M.O. Breckwoldt, et al., Multiparametric optical analysis of mitochondrial redox signals during neuronal physiology and pathology in vivo, Nat. Med. 20 (2014) 555–560, https://doi.org/10.1038/nm.3520.
[22] F.J. Bock, S.W.G. Tait, Mitochondria as multifaceted regulators of cell death, Nat. Rev. Mol. Cell Biol. 21 (2020) 85–100, https://doi.org/10.1038/s41580-019-0173-8.
[23] A.M. Battaglia, et al., Ferroptosis and cancer: mitochondria meet the "iron maiden" cell death, Cells 9 (2020), https://doi.org/10.3390/cells9061505.
[24] B. Gan, Mitochondrial regulation of ferroptosis, J. Cell Biol. 220 (2021), https://doi.org/10.1083/jcb.202105043.
[25] R. Iwata, et al., Mitochondria metabolism sets the species-specific tempo of neuronal development, Science 379 (2023), eabn4705, https://doi.org/10.1126/science.abn4705.

[26] F.A. Rahman, J. Quadrilatero, Mitochondrial network remodeling: an important feature of myogenesis and skeletal muscle regeneration, Cell. Mol. Life Sci. 78 (2021) 4653–4675, https://doi.org/10.1007/s00018-021-03807-9.
[27] A. Roca-Portoles, S.W.G. Tait, Mitochondrial quality control: from molecule to organelle, Cell. Mol. Life Sci. 78 (2021) 3853–3866, https://doi.org/10.1007/s00018-021-03775-0.
[28] M. Guo, et al., Inhibition of ferroptosis promotes retina ganglion cell survival in experimental optic neuropathies, Redox Biol. 58 (2022) 102541, https://doi.org/10.1016/j.redox.2022.102541.
[29] S. Zhong, et al., Energy stress modulation of AMPK/FoxO3 signaling inhibits mitochondria-associated ferroptosis, Redox Biol. 63 (2023) 102760, https://doi.org/10.1016/j.redox.2023.102760.
[30] C.Y. Chang, M.Z. Liang, L. Chen, Current progress of mitochondrial transplantation that promotes neuronal regeneration, Transl. Neurodegener. 8 (2019) 17, https://doi.org/10.1186/s40035-019-0158-8.
[31] J.L. Gollihue, et al., Effects of mitochondrial transplantation on bioenergetics, cellular incorporation, and functional recovery after spinal cord injury, J. Neurotrauma 35 (2018) 1800–1818, https://doi.org/10.1089/neu.2017.5605.
[32] D. Han, et al., Mesenchymal stem/stromal cell-mediated mitochondrial transfer and the therapeutic potential in treatment of neurological diseases, Stem Cells Int 2020 (2020) 8838046, https://doi.org/10.1155/2020/8838046.
[33] C. Li, et al., Temporal and spatial cellular and molecular pathological alterations with single-cell resolution in the adult spinal cord after injury, Signal Transduct. Targeted Ther. 7 (2022) 65, https://doi.org/10.1038/s41392-022-00885-4.
[34] C. Donohoe, M.O. Senge, L.G. Arnaut, L.C. Gomes-da-Silva, Cell death in photodynamic therapy: from oxidative stress to anti-tumor immunity, Biochim Biophys Acta Rev Cancer 1872 (2019) 188308, https://doi.org/10.1016/j.bbcan.2019.07.003.
[35] L. Gong, et al., Spatiotemporal dynamics of the molecular expression pattern and intercellular interactions in the glial scar response to spinal cord injury, Neurosci. Bull. 39 (2023) 213–244, https://doi.org/10.1007/s12264-022-00897-8.
[36] H.M. Ni, J.A. Williams, W.X. Ding, Mitochondrial dynamics and mitochondrial quality control, Redox Biol. 4 (2015) 6–13, https://doi.org/10.1016/j.redox.2014.11.006.
[37] S. Pickles, P. Vigie, R.J. Youle, Mitophagy and quality control mechanisms in mitochondrial maintenance, Curr. Biol. 28 (2018) R170–R185, https://doi.org/10.1016/j.cub.2018.01.004.
[38] B. Zhou, et al., Ferroptosis is a type of autophagy-dependent cell death, Semin. Cancer Biol. 66 (2020) 89–100, https://doi.org/10.1016/j.semcancer.2019.03.002.
[39] J. Liu, et al., Autophagy-dependent ferroptosis: machinery and regulation, Cell Chem. Biol. 27 (2020) 420–435, https://doi.org/10.1016/j.chembiol.2020.02.005.
[40] R. Stavely, K. Nurgali, The emerging antioxidant paradigm of mesenchymal stem cell therapy, Stem Cells Transl Med 9 (2020) 985–1006, https://doi.org/10.1002/sctm.19-0446.
[41] Y.C. Hsu, Y.T. Wu, T.H. Yu, Y.H. Wei, Mitochondria in mesenchymal stem cell biology and cell therapy: from cellular differentiation to mitochondrial transfer, Semin. Cell Dev. Biol. 52 (2016) 119–131, https://doi.org/10.1016/j.semcdb.2016.02.011.
[42] B.R. Stockwell, Ferroptosis turns 10: emerging mechanisms, physiological functions, and therapeutic applications, Cell 185 (2022) 2401–2421, https://doi.org/10.1016/j.cell.2022.06.003.
[43] Y. Chen, et al., The latest view on the mechanism of ferroptosis and its research progress in spinal cord injury, Oxid Med Cell Longev 2020 (2020) 6375938, https://doi.org/10.1155/2020/6375938.
[44] W.D. Bao, et al., Loss of ferroportin induces memory impairment by promoting ferroptosis in Alzheimer's disease, Cell Death Differ. 28 (2021) 1548–1562, https://doi.org/10.1038/s41418-020-00685-9.
[45] C.L. Hu, et al., Reduced expression of the ferroptosis inhibitor glutathione peroxidase-4 in multiple sclerosis and experimental autoimmune encephalomyelitis, J. Neurochem. 148 (2019) 426–439, https://doi.org/10.1111/jnc.14604.
[46] J.N. Cobley, M.L. Fiorello, D.M. Bailey, 13 reasons why the brain is susceptible to oxidative stress, Redox Biol. 15 (2018) 490–503, https://doi.org/10.1016/j.redox.2018.01.008.
[47] M. Gao, et al., Role of mitochondria in ferroptosis, Mol. Cell. 73 (2019) 354–363, https://doi.org/10.1016/j.molcel.2018.10.042, e353.
[48] P. Mishra, D.C. Chan, Mitochondrial dynamics and inheritance during cell division, development and disease, Nat. Rev. Mol. Cell Biol. 15 (2014) 634–646, https://doi.org/10.1038/nrm3877.
[49] A.B. Knott, G. Perkins, R. Schwarzenbacher, E. Bossy-Wetzel, Mitochondrial fragmentation in neurodegeneration, Nat. Rev. Neurosci. 9 (2008) 505–518, https://doi.org/10.1038/nrn2417.
[50] Z. Deng, et al., LncRNA SNHG14 promotes OGD/R-induced neuron injury by inducing excessive mitophagy via miR-182-5p/BINP3 axis in HT22 mouse hippocampal neuronal cells, Biol. Res. 53 (2020) 38, https://doi.org/10.1186/s40659-020-00304-4.
[51] F. Yu, et al., Dynamic O-GlcNAcylation coordinates ferritinophagy and mitophagy to activate ferroptosis, Cell Discov 8 (2022) 40, https://doi.org/10.1038/s41421-022-00390-6.
[52] D.G. Nicholls, S.L. Budd, Mitochondria and neuronal survival, Physiol. Rev. 80 (2000) 315–360, https://doi.org/10.1152/physrev.2000.80.1.315.
[53] D. Trigo, C. Avelar, M. Fernandes, J. Sa, E.S.O. da Cruz, Mitochondria, energy, and metabolism in neuronal health and disease, FEBS Lett. 596 (2022) 1095–1110, https://doi.org/10.1002/1873-3468.14298.
[54] O. Kann, R. Kovacs, Mitochondria and neuronal activity, Am. J. Physiol.: Cell Physiol. 292 (2007) C641–C657, https://doi.org/10.1152/ajpcell.00222.2006.
[55] Q. Han, et al., Restoring cellular energetics promotes axonal regeneration and functional recovery after spinal cord injury, Cell Metabol. 31 (2020) 623–641 e628, https://doi.org/10.1016/j.cmet.2020.02.002.
[56] L. Chien, M.Z. Liang, C.Y. Chang, C. Wang, L. Chen, Mitochondrial therapy promotes regeneration of injured hippocampal neurons, Biochim. Biophys. Acta, Mol. Basis Dis. 1864 (2018) 3001–3012, https://doi.org/10.1016/j.bbadis.2018.06.012.
[57] C.V. Borlongan, et al., May the force be with you: transfer of healthy mitochondria from stem cells to stroke cells, J. Cerebr. Blood Flow Metabol. 39 (2019) 367–370, https://doi.org/10.1177/0271678X18811277.
[58] N. Tseng, et al., Mitochondrial transfer from mesenchymal stem cells improves neuronal metabolism after oxidant injury in vitro: the role of Miro1, J. Cerebr. Blood Flow Metabol. 41 (2021) 761–770, https://doi.org/10.1177/0271678X20928147.
[59] Z. Zhang, et al., Mesenchymal stem cell-conditioned medium improves mitochondrial dysfunction and suppresses apoptosis in okadaic acid-treated SH-SY5Y cells by extracellular vesicle mitochondrial transfer, J Alzheimers Dis 78 (2020) 1161–1176, https://doi.org/10.3233/JAD-200686.
[60] L.L. Liau, et al., Treatment of spinal cord injury with mesenchymal stem cells, Cell Biosci. 10 (2020) 112, https://doi.org/10.1186/s13578-020-00475-3.
[61] X. Wang, H.H. Gerdes, Transfer of mitochondria via tunneling nanotubes rescues apoptotic PC12 cells, Cell Death Differ. 22 (2015) 1181–1191, https://doi.org/10.1038/cdd.2014.211.
[62] M.G. Nasoni, et al., Melatonin reshapes the mitochondrial network and promotes intercellular mitochondrial transfer via tunneling nanotubes after ischemic-like injury in hippocampal HT22 cells, J. Pineal Res. 71 (2021), e12747, https://doi.org/10.1111/jpi.12747.
[63] Y. Li, et al., Microglia-organized scar-free spinal cord repair in neonatal mice, Nature 587 (2020) 613–618, https://doi.org/10.1038/s41586-020-2795-6.
[64] C.P. Hofstetter, et al., Marrow stromal cells form guiding strands in the injured spinal cord and promote recovery, Proc. Natl. Acad. Sci. U. S. A. 99 (2002) 2199–2204, https://doi.org/10.1073/pnas.042678299.
[65] J.L. Liu, et al., Intraperitoneally delivered mesenchymal stem cells alleviate experimental colitis through THBS1-mediated induction of IL-10-competent regulatory B cells, Front. Immunol. 13 (2022), https://doi.org/10.3389/fimmu.2022.853894. ARTN 853894.
[66] M.H. Jiang, et al., Characterization of Nestin-positive stem Leydig cells as a potential source for the treatment of testicular Leydig cell dysfunction, Cell Res. 24 (2014) 1466–1485, https://doi.org/10.1038/cr.2014.149.
[67] H. Ke, et al., Derivation, characterization and gene modification of cynomolgus monkey mesenchymal stem cells, Differentiation 77 (2009) 256–262, https://doi.org/10.1016/j.diff.2008.09.021.
[68] X. Huang, et al., Fast, long-term, super-resolution imaging with Hessian structured illumination microscopy, Nat. Biotechnol. 36 (2018) 451–459, https://doi.org/10.1038/nbt.4115.
[69] D.M. Basso, et al., Basso Mouse Scale for locomotion detects differences in recovery after spinal cord injury in five common mouse strains, J. Neurotrauma 23 (2006) 635–659, https://doi.org/10.1089/neu.2006.23.635.
[70] F. Gong, et al., Trehalose inhibits ferroptosis via NRF2/HO-1 pathway and promotes functional recovery in mice with spinal cord injury, Aging (Albany NY) 14 (2022) 3216–3232, https://doi.org/10.18632/aging.204009.
[71] Q.Z. Tuo, et al., Thrombin induces ACSL4-dependent ferroptosis during cerebral ischemia/reperfusion, Signal Transduct. Targeted Ther. 7 (2022) 59, https://doi.org/10.1038/s41392-022-00917-z.
[72] R. Sugimura, et al., Noncanonical wnt signaling maintains hematopoietic stem cells in the niche, Cell 150 (2012) 351–365, https://doi.org/10.1016/j.cell.2012.05.041.